Spring 5-31-2015

Development of a finite element method for light activated polymers

Craig Hamel
New Jersey Institute of Technology

Copyright Warning & Restrictions

The copyright law of the United States (Title 17, United States Code) governs the making of photocopies or other reproductions of copyrighted material.

Under certain conditions specified in the law, libraries and archives are authorized to furnish a photocopy or other reproduction. One of these specified conditions is that the photocopy or reproduction is not to be "used for any purpose other than private study, scholarship, or research." If a, user makes a request for, or later uses, a photocopy or reproduction for purposes in excess of "fair use" that user may be liable for copyright infringement,

This institution reserves the right to refuse to accept a copying order if, in its judgment, fulfillment of the order would involve violation of copyright law.

Please Note: The author retains the copyright while the New Jersey Institute of Technology reserves the right to distribute this thesis or dissertation

Printing note: If you do not wish to print this page, then select "Pages from: first page # to: last page #" on the print dialog screen

ABSTRACT

DEVELOPMENT OF A FINITE ELEMENT METHOD FOR LIGHT ACTIVATED POLYMERS

by
Craig Hamel

Traditional Shape Memory Polymers (SMPs) belong to a class of smart materials which have shown promise for a wide range of applications. They are characterized by their ability to maintain a temporary deformed shape and return to an original parent permanent shape. The first SMPs developed responded to changes in temperature by exploiting the difference in modulus and chain mobility through the glass transition temperature. However, in recent years, new SMPs have been developed that respond to other stimuli besides temperature; these can include electricity, magnetism, changes in chemical concentration, and even light.

In this thesis, we consider the photo-mechanical behavior of Light Activated Shape Memory Polymers (LASMPs), focusing on the numerical aspects. The mechanics behind LASMPS is rather abstract and cumbersome, even for simple geometries. In order to move these materials out of the lab and into the more modern engineering design framework of commercial design and engineering software, robust numerical methods must be developed in order to implement sound and accurate simulations.

The photo-mechanical theory is summarized and some constitutive laws that govern LASMPS are described. Implementation of the multiphysics governing equations takes the form of a user defined element subroutine within the commercial software package ABAQUS/STANDARD. Simulations are carried out with varied geometries and symmetries, for example plane-strain, axisymmetric, and three-dimensional geometries under complex photo-mechanical loadings.

DEVELOPMENT OF A FINITE ELEMENT METHOD FOR LIGHT ACTIVATED POLYMERS

by
Craig Hamel

A Thesis
Submitted to the Faculty of
New Jersey Institute of Technology
in Partial Fulfillment of the Requirements for the Degree of
Master of Science in Mechanical Engineering

Department of Mechanical and Industrial Engineering

May 2015

APPROVAL PAGE

DEVELOPMENT OF A FINITE ELEMENT METHOD FOR LIGHT ACTIVATED POLYMERS

Craig Hamel

Shawn A. Chester, Thesis Advisor — Date
Assistant Professor of Mechanical and Industrial Engineering, NJIT

I. Joga Rao, Committee Member — Date
Professor of Mechanical and Industrial Engineering, NJIT

Pushpendra Singh, Committee Member — Date
Professor of Mechanical and Industrial Engineering, NJIT

BIOGRAPHICAL SKETCH

Author: Craig Hamel

Degree: Master of Science

Date: May 2015

Undergraduate and Graduate Education:

- Master of Science in Mechanical Engineering
  New Jersey Institute of Technology, Newark, NJ, 2015
- Bachelor of Science in Physics
  The University of Mississippi, Oxford Mississippi, 2012

Major: Mechanical Engineering

Presentations and Publications:

Craig Hamel and Shawn A. Chester, "Modeling light active shape memory polymers," *Submitted*, Society of Engineering Science Annual Technical Meeting, Texas A&M University, 2015.

To my family and The Storms

ACKNOWLEDGMENT

I would like to thank most of all my advisor Dr. Shawn Chester for the wealth of knowledge he bestowed upon me during the course of this work. Thanks are also in order for Dr. I. Joga Rao for allowing us to numerically implement his previous works. Without Dr. Pushpendra Singh's directive to use the SUPG finite element method this work would not have been possible. Finally, I would like to thank Lizzy Storm for her comments and the continuum mechanics illustrations.

TABLE OF CONTENTS

TABLE OF CONTENTS
(Continued)

Chapter **Page**

LIST OF TABLES

Table **Page**

LIST OF FIGURES

CHAPTER 1

INTRODUCTION

1.1 Motivation

The motivation for this work is to formulate a robust finite element implementation that can numerically solve problems which involve the coupling of the physics of large deformable solids and their interaction with light. With this implementation, engineers would have access to a tool which would aid in the design of a new form of smart materials that are responsive to light. One specific example is Light Activated Shape Memory Polymers (LASMPs). LASMPs are different from traditional Shape Memory Polymers (SMPs) in that instead of responding to thermal changes these SMPs respond to particular wavelengths of light.

1.2 The Finite Element Method

The finite element method (FEM) is a way of solving partial differential equations (PDEs) numerically that is especially well suited for complex geometries and computational mechanics. The general idea of the FEM is to formulate a weak form from the governing PDE (or PDEs) along with its boundary conditions (BCs). The development of the weak form involves multiplying the governing PDE by a special mathematical entity known as a weighting function. Once multiplied the result is integrated over the whole body in question. At this point the geometry is then discretized, and the weighting function and solution variables are interpolated using shape functions. Nodes and simple shapes such as triangles and quadrilaterals now make up the previously complex geometry.

The discretization allows the PDE to be converted into a system of nonlinear algebraic equations. Once the problem has been formulated in this setting, a solution

may be obtained using either an implicit Newton-Raphson method, or an explicit incremental method.

1.3 Continuum Mechanics

The modern theory of continuum mechanics offers a unified nonlinear framework between the mechanics and thermodynamics of continua. Emphasis on the fact that this theory is nonlinear is very important to development of constitutive models to describe the states of deformation and stress for different classes of materials.

Constitutive models developed for LASMPs by [22] and [16] will enter into the coupled finite element framework. The general idea behind these models is that the Cauchy stress is the sum of the stresses in each polymer network. The evolution of the network fraction will be coupled to a reaction rate which is driven by the light intensity within the material.

1.4 Shape Memory Polymers (SMPs)

Shape memory polymers have been under development over the past few decades and are a recent addition to the general class of polymeric materials. These polymers are distinct from the rest of polymeric materials since they possess the shape memory property which allows the material to store a temporary shape (which is deformed from the original permanent shape by a form of environmental stimuli), and return to it's permanent shape once the environmental factors have been removed. These stimuli can include fluctuations in temperature, electricity, magnetism, and light. Thermal SMPs were among some of the first of this class of material to be studied such as in [3]. Other than thermal effects [4] have shown polymers can also exhibit the shape memory effect due to chemical, electrical, magnetic, and light. Light activated shape memory polymers will be the concentration of this work, however many of the

ideas presented here can be extended to the study of SMPs which exhibit the shape memory effect due to different physical stimuli.

One of the first widespread applications of thermally activated SMPs were heat shrinkable tubes as discussed in [20]. SMPs are now beginning to be used in critical biomedical applications which require more accurate design techniques to be used safely, e.g. [15], [18], and [1]. Other interesting applications include self-deployable space structures, mircosystems (e.g. [17] and [19]), and re-writable data storage (e.g. [25] and [26]). Technologies with complex geometries, such as those mentioned above, require a validated numerical implementation of a mechanical constitutive theory which is coupled with the environmental stimulus which is the cause of the shape memory affect.

Significant effort in the thermo-mechanical constitutive modelling of thermal SMPs has been published in the literature (e.g. [6], [21], and [24]). There is, however, no widely agreed upon theory for modeling the response of thermal SMPs. Even though the models are not completely accurate, the numerical implementation of these models can promote the development of critical applications.

1.4.1 Light Activated Shape Memory Polymers (LASMPs)

LASMPs have an inherently different mechanism which controls the shape memory effect versus the physical mechanisms of thermally actuated SMPs. Thermal SMPs exploit a phase change that occurs in these polymers once heated above the glass transition temperature, ϑ_g. LASMPs still have an elastomer base but are infused with photo-responsive functional groups that, when exposed to the proper wavelength of light, form new covalent bonds between the main polymer chain. The newly formed bonds are photo-reversible and, upon exposure to a different wavelength, will cleave.

CHAPTER 2

BACKGROUND THEORY

2.1 Continuum Mechanics

The necessary theory from Continuum Mechanics will now be presented in order to numerically implement the conservation of linear momentum alongside the Beer-Lambert law. The notation that will be used is standard of modern continuum mechanics [9]. Specifically: ∇ and Div denote the gradient and divergence with respect to the material point $\mathbf{X}$ in the reference configuration; grad and div denote these operators with respect to the point $\mathbf{x} = \boldsymbol{\chi}(\mathbf{X}, t)$ in the deformed body; a superposed dot denotes the material time-derivative. Boldface capital letters, such as $\mathbf{A}$, will denote tensor quantities, boldface lower case letters will represent vector quantities, such as $\mathbf{a}$, and lowercase Greek letters will be used to denote scalar quantities, such as α. Also $\mathcal{B}_{\mathrm{R}}$ and $\mathcal{B}_t$ will denote a material body and spatial body respectively and $\mathcal{S}$ will be used to denote the surface of a spatial body $\mathcal{B}_t$. Throughout, $\mathbf{F}^{-1} = (\mathbf{F})^{-1}$, $\mathbf{F}^{-\top} = (\mathbf{F})^{-\top}$, etc. Some more tensor notation includes $\operatorname{tr}\mathbf{A}$, $\operatorname{sym}\mathbf{A}$, $\operatorname{skw}\mathbf{A}$, $\mathbf{A}_0$, and $\operatorname{sym}_0\mathbf{A}$ respectively, for the trace, symmetric, skew, deviatoric, and symmetric-deviatoric parts of a tensor $\mathbf{A}$. Also, the inner product of tensors $\mathbf{A}$ and $\mathbf{B}$ is denoted by $\mathbf{A}:\mathbf{B}$, and the magnitude of $\mathbf{A}$ by $|\mathbf{A}| = \sqrt{\mathbf{A}:\mathbf{A}}$. For a more detailed introduction to modern continuum mechanics, see [9] and [10].

2.1.1 General Kinematics

Let $\mathcal{B}_{\mathrm{R}}$ denote the continuous region of space that a body of material occupies in a fixed reference configuration, and denote a material point by $\mathbf{X}$. $\mathcal{B}_t$ will denote the region that the material body occupies during a specific time $t > 0$, a spatial point in this region will be denoted by $\mathbf{x}$. Now define the function $\boldsymbol{\chi}$ which maps material

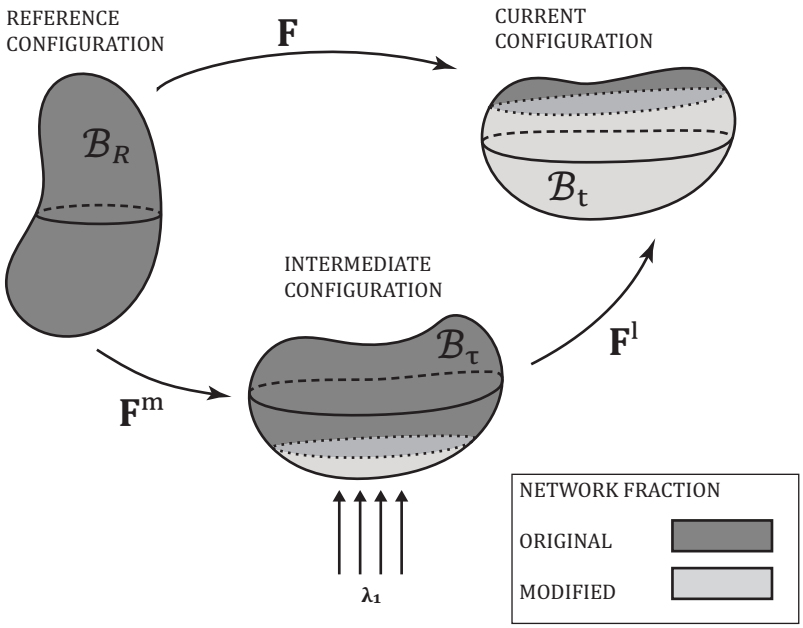

Figure 2.1 Schematic of configurations involved in the formation and dissolution of the second polymer network.

points to spatial ones

$$\mathbf{x} = \boldsymbol{\chi}(\mathbf{X}, t). \tag{2.1}$$

The deformation gradient is defined as

$$\mathbf{F} = \frac{\partial \boldsymbol{\chi}}{\partial \mathbf{X}}, \tag{2.2}$$

and the left and right Cauchy-Green stretch tensors are defined as

$$\mathbf{B} = \mathbf{F}\mathbf{F}^{\top}, \tag{2.3}$$

$$\mathbf{C} = \mathbf{F}^{\top}\mathbf{F}. \tag{2.4}$$

2.1.2 Kinematics of LASMPS

For LASMPs, multiple natural configurations are necessary to describe the complex nature of the problem. Let $\mathcal{B}_{\mathrm{R}}$ denote the reference configuration and let $\mathcal{B}_t$ represent

the current configuration respectively. Now define an intermediate space $\mathcal{B}_\tau$ that corresponds to the body when exposed to light, when the new polymer network is formed atop the previous. The introduction of the intermediate configuration allows for the decomposition of the deformation gradient, see Figure 2.1, as follows

$$\mathbf{F}^l = \mathbf{F}\mathbf{F}^{m-1} \tag{2.5}$$

where $\mathbf{F}^m$ corresponds to the mechanical component of the motion prior to exposure to light, and $\mathbf{F}^l$ corresponds to the motion of the second network after exposure to light. Keep in mind that the original network deformation is always measured from the reference configuration $\mathcal{B}_{\mathrm{R}}$. This decomposition will aid in the numerical implementation of the shape memory constitutive response.

2.1.3 Conservation Laws

The conservation laws of continuum mechanics will be necessary within the theoretical framework as well as the numerical one. The standard laws of conservation of mass and linear momentum will be presented for the eventual numerical implantation. The conservation laws are as follows

$$\dot{\rho} + \rho \mathrm{div}(\mathbf{v}) = 0 \tag{2.6}$$

$$\rho\dot{\mathbf{v}} = \mathrm{div}\mathbf{T} + \mathbf{b}_0 \tag{2.7}$$

where Equation (2.6) is the conservation of mass and Equation (2.7) is the conservation of linear momentum. For simplicity steady-state problems will be considered, $\dot{\mathbf{v}} = 0$, and body forces will be neglected; $\mathbf{b}_0 = \mathbf{0}$. Thus the balance of linear momentum will take the following form

$$\mathrm{div}\mathbf{T} = \mathbf{0} \tag{2.8}$$

2.1.4 General Constitutive Models

In order to fully close the conservation of linear momentum, a constitutive relation for the Cauchy stress $\mathbf{T}$ must be defined. The LASMP can be modeled as an elastomeric polymer which can be achieved using several material models such as the Neo-Hookean, Mooney-Rivlin, or the Arruda-Boyce models. In this work, the Neo-Hookean model will be used due to its simplicity. For each network i, the Neo-Hookean stress is given as

$$\mathbf{T}_i = \mu_i \left(\mathbf{B}_{\text{dis}_i}\right)_0 + K_i(\ln J_i)\mathbf{1} \tag{2.9}$$

where μ_i is the shear modulus of network i, $\mathbf{B}_{\text{dis}_i} = J_i^{-2/3}\mathbf{B}_i$, $(\mathbf{B}_{\text{dis}_i})_0 = \mathbf{B}_{\text{dis}_i} - \frac{1}{3}\text{tr}\,\mathbf{B}_{\text{dis}_i}$ and K_i is the bulk modulus of network i. Then for a two network polymer the total stress is

$$\mathbf{T} = (1-\alpha)\mathbf{T}_1 + \alpha\mathbf{T}_2 \tag{2.10}$$

where α $(0 \leq \alpha \leq 1)$ is the fraction of the newly formed network, $\mathbf{T}_1$ is the stress in the original network, and $\mathbf{T}_2$ is the stress in the newly formed network. Therefore for $\alpha = 1$ there is no presence of the second network and all of the stress is in the original network. In general a constitutive relation is necessary for the evolution of α, both during the formation and dissolution of the second network, which is coupled to the light intensity through photochemical reactions. Relations of this form are given in [23] for the evolution of α under homogeneous light intensity which implies that the extent of the reaction is homogeneous throughout the body. The evolution of α while the second network is forming is given by

$$\dot{\alpha} = k_f(1-\alpha)^n \tag{2.11}$$

where k_f is the rate constant of the forward reaction and n is the order of the reaction. The evolution of α during the dissolution of the second network is given by

$$\dot{\alpha} = -k_r \alpha^n \tag{2.12}$$

where again n is the order of the reaction and k_r is the rate constant of the reverse reaction.

These relations are reasonably valid for optically thin members. In this work however, the evolution of α will be coupled to the photochemical reactions of specific light activated polymers that are optically thick. This will induce an inhomogeneous extent of the reaction throughout the material which will cause an inhomogeneous shape memory recovery.

2.2 Photo-Mechanics

This section will present the necessary theory for describing the mechanism by which light penetrates and transmits through a continuous solid material. Radiative transfer will be presented and several simplifying assumptions will be made on the governing equations. This will lead to the well known Beer-Lambert law which will define the strong form of the mechanism by which light interacts with deformable matter within the uncoupled as well as the coupled theory.

2.2.1 Radiative Transfer

Radiative transfer is the method by which light transfers energy through a continuous medium. As light travels, photons will transport electromagnetic energy through various mechanisms such as, scattering, emission, and absorption. The governing equation for radiative transfer is (see [5])

$$\frac{1}{c}\frac{\partial I}{\partial t} + \mathbf{d} \cdot \operatorname{grad} I + (k_s + k_a) I = j + \frac{1}{4\pi c} k_s \int_\Omega I d\Omega \tag{2.13}$$

where c is the speed of light, $\mathbf{d}$ is the local direction that light is propagating , I is the specific light intensity, k_s is the scattering coefficient, k_a is the absorption coefficient, and j is the emission coefficient. The integral takes into account the scattered light.

If scattering and emission are neglected which for some LASMPs have been shown to be negligible by [2], then the resulting equation is

$$\mathbf{d} \cdot \operatorname{grad} I + \sigma I = 0 \tag{2.14}$$

In order to make the boundary value problem (BVP) well posed, appropriate boundary conditions (BCs) must be defined. This particular equation belongs to a class of PDEs known as first-order hyperbolic PDEs which exhibit boundaries of the form

$$\mathcal{S} = \mathcal{S}_- \cup \mathcal{S}_+ \tag{2.15}$$

where

$$\mathcal{S}_- = \{\mathbf{x} \in \mathcal{S} \mid \mathbf{d}(\mathbf{x}) \cdot \mathbf{n}(\mathbf{x}) < 0\} \tag{2.16}$$

and

$$\mathcal{S}_+ = \{\mathbf{x} \in \mathcal{S} \mid \mathbf{d}(\mathbf{x}) \cdot \mathbf{n}(\mathbf{x}) > 0\}. \tag{2.17}$$

The boundary condition of Beer's law is defined only on $\mathcal{S}_-$ and not the entirety of the boundary due to the first order nature of the problem. The BC is a prescribed light intensity on $\mathcal{S}_-$, i.e. $I = I_0$. The BVP is then defined as

$$\begin{cases} \mathbf{d} \cdot \operatorname{grad} I + \sigma I = 0 \quad \text{in } \mathcal{B}_t \\ \qquad\qquad\qquad I = I_0 \quad \text{on } \mathcal{S}_- \end{cases} \tag{2.18}$$

which will act as the governing equation for describing the light intensity in the numerical implementation.

2.3 Photochemistry

The photochemistry of two recently developed classes of LASMPs will be discussed briefly in this section to highlight the process of how to couple the polymer fraction to specific polymeric constituents. First the class of LASMPs with photo-tunable molecular crosslinks (PMC), which is the simpler of the two, will be discussed; followed by LASMPs whose shape-memory affect is governed by photo-tunable network rearrangement (PNR). These two classes of LASMPs are discussed at length in [16].

2.3.1 PMC Material

Recently an amorphous polymer with photo-tunable molecular crosslinks (PMC) was developed, see [13] and [14]. The rate of reaction for a PMC material is governed by the bonding and cleaving of chromophores. Let C_{UB} represent the concentration of unbonded chromophore pairs and let C_B be the concentration of bonded chromophore pairs, where in general C_{UB} and C_B are functions of position and time.

$$\begin{cases} \dfrac{\partial C_{UB}}{\partial t} = -\left(\frac{\phi_{UB}\alpha_{UB}}{N_A h\nu}\right) C_{UB}^2 I + 2\left(\frac{\phi_B \alpha_B}{N_A h\nu}\right) C_B I, & \text{in } \mathcal{B}_t. \\ C_{UB} = C_0, & \text{for } t = 0. \\ C_{UB} + 2C_B = C_0, & \text{for } t \geq 0. \end{cases} \tag{2.19}$$

where N_A is Avogadro's number, h is Planck's constant, ν is the frequency of the light driving the reaction, α_{UB} and α_B are the absorptivities of unbonded and bonded chomophores respectively, ϕ_{UB} and ϕ_B are the quantum efficiencies of the bonding and cleaving of chromophores which can be a function of frequency in the range 0 to 1. For simplicity they will be defined as follows for bonding

$$\phi_{UB} = 1, \text{ and } \phi_B = 0, \text{ for } \nu > \nu_c \tag{2.20}$$

and for the cleaving of chromophore bonds.

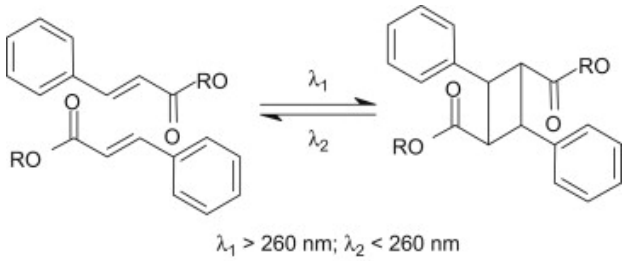

Figure 2.2 PMC reaction showcasing the formation of molecular cross links between chromophores. Image from [16].

$$\phi_{UB} = 0, \text{ and } \phi_B = 1, \text{ for } \nu > \nu_c \tag{2.21}$$

For a PMC material the evolution of the polymer fraction is defined as

$$\begin{cases} \alpha = k_2 C_B & \text{for } t \geq 0 \\ \alpha = 0 & \text{for } t = 0 \end{cases} \tag{2.22}$$

CHAPTER 3

FINITE ELEMENT FORMULATION

In the absence of body forces, the strong forms of the governing PDEs are

$$\left.\begin{array}{l}\text{Balance of momentum} \left\{\begin{array}{rl} \operatorname{div}\mathbf{T} = \mathbf{0} & \text{in } \mathcal{B}_t, \\ \mathbf{u} = \breve{\mathbf{u}} & \text{on } \mathcal{S}_{\mathbf{u}}, \\ \mathbf{T}\mathbf{n} = \breve{\mathbf{t}} & \text{on } \mathcal{S}_{\mathbf{t}}, \end{array}\right. \\ \text{Radiative Transfer} \left\{\begin{array}{rl} \mathbf{d}\cdot\operatorname{grad} I + \sigma I = 0, & \text{in } \mathcal{B}_t, \\ I = I_0 & \text{on } \mathcal{S}_-\end{array}\right.\end{array}\right\} \tag{3.1}$$

where above $\partial\mathcal{S} = \mathcal{S}_{\mathbf{u}} \cup \mathcal{S}_{\mathbf{t}}$, $\mathcal{S}_{\mathbf{u}} \cap \mathcal{S}_{\mathbf{t}} = \emptyset$ and

$$\mathcal{S}_- = \{\mathbf{x} \in \partial\mathcal{S} \mid \mathbf{n}(\mathbf{x})\cdot\mathbf{d} < 0\} \tag{3.2}$$

where $\mathbf{n}(\mathbf{x})$ is the normal vector to the surface $\mathcal{S}$ at the point $\mathbf{x}$ on $\mathcal{S}$. The process of numerical formulation will ensue as follows:

- The usual Galerkin form of the weak problem will be derived for the Beer-Lambert Law, however this approach leads to a non-stable method for this particular class of problems.
- To stabilize the problem a Streamline-Upwind Petrov Galerkin (SUPG) form of the problem, with some artificial diffusion added, will be derived in order to improve the error bounds of the solutions.
- Once the uncoupled photo-chemical theory has been verified, a photo-mechanical constitutive model is implemented into a coupled multiphysics finite element implementation.

3.1 Galerkin Formulation of the Beer-Lambert Law

This section presents the standard approach to formulating a Galerkin weak form from the corresponding strong form. The BVP is

$$\begin{cases} \mathbf{d} \cdot \operatorname{grad} I + \sigma I = 0 \text{ in } \mathcal{B}_t \\ I = I_0, \text{ on } \mathcal{S}_- \end{cases} \tag{3.3}$$

where $\mathbf{d}$, a unit vector, represents the direction of light incidence, I is the light intensity, I_0 is the initial light intensity, and σ is the absorptivity of the given material. In order to formulate the weak form, the strong form will be multiplied by a sufficiently continuously differentiable scalar test function w_1 and integrated over the body $\mathcal{B}_t$, which gives

$$\int_{\mathcal{B}_t} w_1 \mathbf{d} \cdot \operatorname{grad} I dv + \int_{\mathcal{B}_t} w_1 \sigma I dv = 0 \tag{3.4}$$

The body $\mathcal{B}_t$ is approximated using finite elements such that $\mathcal{B}_t = \cup \mathcal{B}_t^e$ and the light intensity field is interpolated inside each element by

$$I = \sum I^A N^A \tag{3.5}$$

where the index $A = 1, 2, ..., M$ is used to denote the nodes of the element, I^A is used to represent the nodal values of light intensity, N^A are the shape functions; to be discussed later. For the standard Galerkin approach the weighting field w_1 is interpolated as follows

$$w_1 = \sum w_1^A N^A \tag{3.6}$$

upon inserting the above interpolants into Equation (3.4) gives

$$\int_{\mathcal{B}_t^e} w_1^A N^A \mathbf{d} \cdot \operatorname{grad} I dv + \int_{\mathcal{B}_t^e} w_1^A N^A \sigma I dv = 0, \tag{3.7}$$

which may be simplified to

$$w_1^A \left(\int_{\mathcal{B}_t^e} N^A \mathbf{d} \cdot \operatorname{grad} I dv + \int_{\mathcal{B}_t^e} N^A \sigma I dv \right) = 0. \tag{3.8}$$

Now, since the w_1^A's factor out, and since they are arbitrary, we define the residual vector for light intensity at each node "A" as

$$R_I^A = \int_{\mathcal{B}_t^e} N^A \mathbf{d} \cdot \operatorname{grad} I dv + \int_{\mathcal{B}_t^e} N^A \sigma I dv = 0. \tag{3.9}$$

Along with the corresponding tangent required for the iterative Newton solver

$$\begin{aligned} K_{II}^{AB} &= -\frac{\partial R_I^A}{\partial I^B} \\ &= -\frac{\partial}{\partial I^B} \int_{\mathcal{B}_t^e} N^A \mathbf{d} \cdot \operatorname{grad} I dv - \frac{\partial}{\partial I^B} \int_{\mathcal{B}_t^e} N^A \sigma I dv \\ &= -\int_{\mathcal{B}_t^e} N^A \mathbf{d} \cdot \frac{\partial}{\partial I^B} \operatorname{grad} I dv - \int_{\mathcal{B}_t^e} \sigma N^A \frac{\partial I}{\partial I^B} dv - \int_{\mathcal{B}_t^e} I N^A \frac{\partial \sigma}{\partial I} dv \end{aligned}$$

making use of the chain rule and using the element wise definition of light intensity $I = I^B N^B$ shows that

$$\frac{\partial}{\partial I^B} \operatorname{grad} I = \operatorname{grad} N^B. \tag{3.10}$$

Therefore the final form of the tangent matrix is

$$K_{II}^{AB} = -\int_{\mathcal{B}_t^e} N^A \mathbf{d} \cdot \operatorname{grad} N^B dv - \int_{\mathcal{B}_t^e} N^A \sigma N^B dv - \int_{\mathcal{B}_t^e} N^A I \frac{\partial \sigma}{\partial I} N^B dv \tag{3.11}$$

or in index notation

$$K_{II}^{AB} = -\int_{\mathcal{B}_t^e} N^A d_i \frac{\partial N^B}{\partial x_i} dv - \int_{\mathcal{B}_t^e} N^A \sigma N^B dv - \int_{\mathcal{B}_t^e} N^A I \frac{\partial \sigma}{\partial I} N^B dv \tag{3.12}$$

Note that the term $\frac{\partial \sigma}{\partial I}$ in the previous equation represents material non-linearity. This is useful for simulating materials in which the absorptivity of the material is highly dependent upon the light intensity.

However this formulation is not a sufficient numerical scheme for the given class of equations. This method will lead to oscillatory solutions and must be stabilized. This will be accomplished by the addition of a small amount of artificial diffusion and using a more sophisticated form of the weighting function which will put more weight on the direction in which the light travels. This method of formulation is known as the Streamline Upwind Petrov-Galerkin (SUPG) formulation. It should be noted that the SUPG does not necessitate the addition of artificial diffusion however, we have found it helps to obtain converged solutions in ABAQUS.

3.2 Streamline Upwind Petrov-Galerkin Formulation (SUPG)

Due to the well known numerical difficulties of first order hyperbolic PDEs a different approach other than the standard Galerkin method must be utilized. First artificial diffusion will be added to the strong form of the problem in order to smooth out the noisy solutions exhibited by the Galerkin formulation. The other change will be in the form of the weighting functions used to develop the weak form. The new BVP reads as

$$\text{Modified Strong From} \begin{cases} \operatorname{div}(\epsilon \operatorname{grad} I) + \mathbf{d} \cdot \operatorname{grad} I + \sigma I = 0, & \text{in } \mathcal{B}_t, \\ I = I_0, & \text{on } \mathcal{S}_-, \\ \epsilon \operatorname{grad} I \cdot \mathbf{n} = 0 & \text{on } \mathcal{S} \setminus \mathcal{S}_-, \end{cases} \tag{3.13}$$

where ϵ is taken to be a very small number, and as $\epsilon \to 0$ the modified strong form will converge to the Beer-Lambert Law. However, we note that since we have raised the order of the PDE, the additional boundary condition is also artificial and will lead to errors that will be addressed in future work. The difference in this formulation compared to the standard Galerkin approach is the choice of the weighting function which is discussed in length in [11]. For the SUPG form we choose a weighting function $\bar{w_1}$ such that $\bar{w_1} = w_1 + \tau \mathbf{d} \cdot \operatorname{grad} w_1$, where w_1 is the weighting function

used in a standard Galerkin scheme and τ is the so called stabilization parameter. This has the effect of putting more influence on the weighting function in the upwind direction, where the information flows from in this class of problems. Now, repeating the procedure, we integrate over the body $\mathcal{B}_t$

$$\int_{\mathcal{B}_t} \bar{w_1} \left(\operatorname{div} \left(\epsilon \operatorname{grad} I \right) + \mathbf{d} \cdot \operatorname{grad} I + \sigma I \right) dv = 0 \tag{3.14}$$

$$\int_{\mathcal{B}_t} \bar{w_1} \operatorname{div} \left(\epsilon \operatorname{grad} I \right) + \int_{\mathcal{B}_t} \bar{w_1} \mathbf{d} \cdot \operatorname{grad} I dv + \int_{\mathcal{B}_t} \bar{w_1} \sigma I dv = 0 \tag{3.15}$$

Now we use the divergence theorem on the first term

$$- \int_{\mathcal{S}} \bar{w_1} \epsilon \operatorname{grad} I \cdot \mathbf{n} da + \int_{\mathcal{B}_t} \epsilon \operatorname{grad} \bar{w_1} \cdot \operatorname{grad} I dv + \int_{\mathcal{B}_t} \bar{w_1} \mathbf{d} \cdot \operatorname{grad} I dv + \int_{\mathcal{B}_t} \bar{w_1} \sigma I dv = 0 \tag{3.16}$$

where $\epsilon \operatorname{grad} I \cdot \mathbf{n} = 0$.

The body $\mathcal{B}_t$ is approximated using finite elements such that $\mathcal{B}_t = \cup \mathcal{B}_t^e$ and the light intensity field is interpolated inside each element by

$$I = \sum I^A N^A \tag{3.17}$$

where the index $A = 1, 2, ..., M$ is used to denote the nodes of the element, I^A is used to represent the nodal values of light intensity, N^A are the shape functions; to be discussed later. For the SUPG formulation the weighting field $\bar{w_1}$ is interpolated as follows

$$\bar{w_1} = \sum \left(w_1^A N^A + w_1^A \tau \mathbf{d} \cdot \operatorname{grad} N^A \right) \tag{3.18}$$

Inserting the above interpolants into Equation (3.16) gives

$$\int_{\mathcal{B}_t^e} \epsilon \text{grad}\left(w_1^A N^A + w_1^A \tau \mathbf{d}\cdot\text{grad}\, N^A\right)\cdot\text{grad}\, I dv + \int_{\mathcal{B}_t^e}\left(w_1^A N^A + w_1^A \tau \mathbf{d}\cdot\text{grad}\, N^A\right)\left(\mathbf{d}\cdot\text{grad}\, I + \sigma I\right) dv = 0, \quad (3.19)$$

which simplifies to

$$w_1^A \int_{\mathcal{B}_t^e} \epsilon\,\text{grad}\, N^A\cdot\text{grad}\, I dv + w_1^A \int_{\mathcal{B}_t^e} \tau\,\text{div}\left(\text{grad}\, N^A\right)\mathbf{d}\cdot\text{grad}\, I dv + w_1^A \int_{\mathcal{B}_t^e} N^A\left(\mathbf{d}\cdot\text{grad}\, I + \sigma I\right) dv + w_1^A \int_{\mathcal{B}_t^e} \tau\left(\mathbf{d}\cdot\text{grad}\, N^A\right)\left(\mathbf{d}\cdot\text{grad}\, I + \sigma I\right) dv = 0. \quad (3.20)$$

Note that $\text{div}\left(\text{grad}\, N^A\right) = 0$ for linear shape functions, also since the the w_1^As factor out and they are arbitrary, the residual vector for light intensity is

$$R_I^A = \int_{\mathcal{B}_t^e} N^A\left(\mathbf{d}\cdot\text{grad}\, I + \sigma I\right) dv + \int_{\mathcal{B}_t^e} \tau\left(\mathbf{d}\cdot\text{grad}\, N^A\right)\left(\mathbf{d}\cdot\text{grad}\, I + \sigma I\right) dv + \int_{\mathcal{B}_t^e} \epsilon\text{grad}\, N^A\cdot\text{grad}\, I dv. \quad (3.21)$$

As before, the corresponding tangent matrix is

$$\begin{aligned} K_{II}^{AB} &= -\frac{\partial R_I^A}{\partial I^B} \\ &= -\frac{\partial}{\partial I^B}\int_{\mathcal{B}_t^e} N^A\left(\mathbf{d}\cdot\text{grad}\, I + \sigma I\right) dv \\ &\quad -\frac{\partial}{\partial I^B}\int_{\mathcal{B}_t^e} \tau\left(\mathbf{d}\cdot\text{grad}\, N^A\right)\left(\mathbf{d}\cdot\text{grad}\, I + \sigma I\right) dv \\ &\quad -\frac{\partial}{\partial I^B}\int_{\mathcal{B}_t^e} \epsilon\text{grad}\, N^A\cdot\text{grad}\, I dv \end{aligned}$$

making use of the chain rule and using the element wise definition of light intensity $I = I^A N^A$ shows that

$$\frac{\partial I}{\partial I^B} = \frac{\partial I}{\partial I}\frac{\partial I}{\partial I^B} = \frac{\partial I}{\partial I^B} = N^B. \quad (3.22)$$

Therefore the final form of the tangent matrix is

$$\begin{aligned} K_{II}^{AB} = &- \int_{\mathcal{B}_t^e} N^A \left(\mathbf{d} \cdot \operatorname{grad} N^B + \sigma N^B + I \frac{\partial \sigma}{\partial I} N^B \right) dv \\ &- \int_{\mathcal{B}_t^e} \tau \left(\mathbf{d} \cdot \operatorname{grad} N^A \right) \left(\mathbf{d} \cdot \operatorname{grad} N^B + \sigma N^B + I \frac{\partial \sigma}{\partial I} N^B \right) \\ &- \int_{\mathcal{B}_t^e} \epsilon \operatorname{grad} N^A \cdot \operatorname{grad} N^B dv, \end{aligned}$$

or in index notation

$$\begin{aligned} K_{II}^{AB} = &- \int_{\mathcal{B}_t^e} N^A \left(d_i \frac{\partial N^B}{\partial x_i} + \sigma N^B + I \frac{\partial \sigma}{\partial I} N^B \right) dv \\ &- \int_{\mathcal{B}_t^e} \tau \left(d_i \frac{\partial N^A}{\partial x_i} \right) \left(d_i \frac{\partial N^B}{\partial x_i} + \sigma N^B + I \frac{\partial \sigma}{\partial I} N^B \right) dv \\ &- \int_{\mathcal{B}_t^e} \epsilon \frac{\partial N^A}{\partial x_i} \frac{\partial I}{\partial x_i} dv. \end{aligned}$$

The SUPG stabilization τ still needs to be defined in order to stabilize the solutions using this particular scheme.

3.3 Large Deformation Weak Form

In this section the weak form will be developed from the strong form for a large deformation continuum theory. For a more in depth discussion of non-linear finite element methods with emphasis on solid mechanics consult [27]. Starting from the strong form

$$\text{Balance of Linear Momentum} \begin{cases} \operatorname{div} \mathbf{T} = \mathbf{0} & \text{in } \mathcal{B}_t, \\ \mathbf{u} = \breve{\mathbf{u}} & \text{on } \mathcal{S}_{\mathbf{u}}, \\ \mathbf{T}\mathbf{n} = \breve{\mathbf{t}} & \text{on } \mathcal{S}_{\mathbf{t}}, \end{cases} \tag{3.23}$$

we introduce a sufficiently continuously differentiable vector weighting function $\mathbf{w}_2$, such that $\mathbf{w}_2 = \mathbf{0}$ on $\mathcal{S}_{\mathbf{u}}$, and we multiply the balance of linear momentum by $\mathbf{w}_2$ and

integrate over the body $\mathcal{B}_t$. This yields

$$\int_{\mathcal{B}_t} \mathbf{w}_2 \mathrm{div}\, \mathbf{T} dv = \mathbf{0} \tag{3.24}$$

$$\int_{\mathcal{B}_t} \mathrm{div}\, (\mathbf{T}\mathbf{w}_2)\, dv - \int_{\mathcal{B}_t} \mathbf{T} : \mathrm{grad}\, \mathbf{w}_2 dv = \mathbf{0} \tag{3.25}$$

using the divergence theorem on the first term of (3.25) gives

$$\int_{\mathcal{S}} (\mathbf{T}\mathbf{w}_2) \cdot \mathbf{n} da - \int_{\mathcal{B}_t} \mathbf{T} : \mathrm{grad}\, \mathbf{w}_2 dv = \mathbf{0} \tag{3.26}$$

where $\mathbf{n}$ is the unit normal vector to the surface $\mathcal{S}$. Furthermore

$$\int_{\mathcal{S}_\mathbf{t}} (\mathbf{T}\mathbf{w}_2) \cdot \mathbf{n} da - \int_{\mathcal{B}_t} \mathbf{T} : \mathrm{grad}\, \mathbf{w}_2 dv = \mathbf{0} \tag{3.27}$$

the last implication is due to the fact that $\mathbf{w}_2$ vanishes on $\mathcal{S}_\mathbf{u}$. Now under the assumption that the Cauchy stress $\mathbf{T}$ is symmetric i.e. $\mathbf{T} = \mathbf{T}^\top$ and the definition of transpose produces

$$\int_{\mathcal{S}_\mathbf{t}} \mathbf{w}_2 \cdot (\mathbf{T}\mathbf{n})\, da - \int_{\mathcal{B}_t} \mathbf{T} : \mathrm{grad}\, \mathbf{w}_2 dv = \mathbf{0} \tag{3.28}$$

now using the boundary condition defined in (3.23)

$$\int_{\mathcal{S}_\mathbf{t}} \mathbf{w}_2 \cdot \breve{\mathbf{t}} da - \int_{\mathcal{B}_t} \mathbf{T} : \mathrm{grad}\, \mathbf{w}_2 dv = \mathbf{0} \tag{3.29}$$

The body $\mathcal{B}_t$ is approximated using finite elements such that $\mathcal{B}_t = \cup \mathcal{B}_t^e$ and the displacement field is interpolated as

$$\mathbf{u} = \sum \mathbf{u}^A N^A \tag{3.30}$$

where the index $A = 1, 2, ..., M$ is used to denote the nodes of the element, I^A is used to represent the nodal values of displacement, N^A are the shape functions; to

be discussed later. For the standard Galerkin formulation the weighting field $\mathbf{w}_2$ is interpolated as follows

$$\mathbf{w}_2 = \sum \mathbf{w}_2^A N^A \tag{3.31}$$

Upon insertion of the above interpolants into Equation (3.29) we obtain

$$\int_{\mathcal{S}_{\mathbf{t}}^e} \mathbf{w}^A N^A \cdot \breve{\mathbf{t}} da - \int_{\mathcal{B}_t^e} \mathbf{T} : \text{grad}\left(\mathbf{w}^A N^A\right) dv = \mathbf{0} \tag{3.32}$$

Now inserting this result into (3.32) gives

$$\int_{\mathcal{S}_{\mathbf{t}}^e} \mathbf{w}^A N^A \cdot \breve{\mathbf{t}} da - \int_{\mathcal{B}_t^e} \mathbf{T}\mathbf{w}^A \text{grad}\, N^A dv = \mathbf{0} \tag{3.33}$$

which in index notation may be expressed as

$$\int_{\mathcal{S}_{\mathbf{t}}^e} w_i^A N^A \breve{t}_i da - \int_{\mathcal{B}_t^e} T_{ij} w_i^A \frac{\partial N^A}{\partial x_j} dv = 0 \tag{3.34}$$

and since w_i^A is constant it can be pulled out of the integrals which gives

$$w_i^A \left(\int_{\mathcal{S}_{\mathbf{t}}^e} N^A \breve{t}_i da - \int_{\mathcal{B}_t^e} T_{ij} \frac{\partial N^A}{\partial x_j} dv \right) = 0 \tag{3.35}$$

and since w_i^A is non-zero and arbitrary on $\mathcal{S}_{\mathbf{t}}^e$ and in $\mathcal{B}_t$ the result is

$$\int_{\mathcal{S}_{\mathbf{t}}^e} N^A \breve{t}_i da - \int_{\mathcal{B}_t^e} T_{ij} \frac{\partial N^A}{\partial x_j} dv = 0 \tag{3.36}$$

The displacement residual $R_{u_i}^A$ will now be defined within the finite element framework as

$$R_{u_i}^A = \int_{\mathcal{S}_{\mathbf{t}}^e} N^A \breve{t}_i da - \int_{\mathcal{B}_t^e} T_{ij} \frac{\partial N^A}{\partial x_j} dv \tag{3.37}$$

Now the tangent matrix $K_{\mathbf{uu}}^{AB}$ can be defined for the deformation problem in index notation using the identities $dv = J dv_{\text{R}}$, the definition of the Kirchhoff stress

$\boldsymbol{\tau} = J\mathbf{T} = \mathbf{T}_{\mathrm{R}}\mathbf{F}^{\top}$, where $\mathbf{T}_{\mathrm{R}}$ is the Piola stress, together with the identity $\mathbf{F}^{-\top}\nabla\varphi = \operatorname{grad}\varphi$ for a scalar field φ, we may recast the residual in the referential form neglecting the first term which is simply the traction boundary condition

$$R^A_{u_i} = -\int_{\mathrm{B}^e} \frac{\partial N^A}{\partial X_a} F^{-1}_{aj} \tau_{ij} dv_{\mathrm{R}}. \tag{3.38}$$

Now using these identities

$$F_{mn} = \delta_{mn} + \sum u^B_m \frac{\partial N^B}{\partial X_n}, \quad \frac{\partial F^{-1}_{ji}}{\partial F_{kl}} = -F^{-1}_{li} F^{-1}_{jk}, \quad \text{and} \quad \frac{\partial N^A}{\partial x_i} = F^{-1}_{ai} \frac{\partial N^A}{\partial X_a},$$

we have

$$\begin{aligned}
K^{AB}_{u_i u_k} &= -\frac{\partial R^A_{u_i}}{\partial u^B_k} \\
&= \int_{\mathrm{B}^e} \frac{\partial N^A}{\partial X_a} \left(\frac{\partial F^{-1}_{aj}}{\partial F_{mn}} \tau_{ij} + F^{-1}_{aj} \frac{\partial \tau_{ij}}{\partial F_{mn}} \right) \frac{\partial F_{mn}}{\partial u^B_k} dv_{\mathrm{R}} \\
&= \int_{\mathrm{B}^e} \frac{\partial N^A}{\partial X_a} \left(\frac{\partial F^{-1}_{aj}}{\partial F_{mn}} \tau_{ij} + F^{-1}_{aj} \frac{\partial \tau_{ij}}{\partial F_{mn}} \right) \frac{\partial N^B}{\partial X_n} \delta_{mk} dv_{\mathrm{R}} \\
&= \int_{\mathrm{B}^e} \frac{\partial N^A}{\partial X_a} \left(-F^{-1}_{nj} F^{-1}_{am} \tau_{ij} + F^{-1}_{aj} \frac{\partial \tau_{ij}}{\partial F_{mn}} \right) \frac{\partial N^B}{\partial X_n} \delta_{mk} dv_{\mathrm{R}} \\
&= \int_{\mathrm{B}^e} \frac{\partial N^A}{\partial X_a} \left(-F^{-1}_{ak} F^{-1}_{nj} \tau_{ij} + F^{-1}_{aj} \frac{\partial \tau_{ij}}{\partial F_{kn}} \right) \frac{\partial N^B}{\partial X_n} dv_{\mathrm{R}} \\
&= \int_{\mathrm{B}^e} \frac{\partial N^A}{\partial x_j} F_{ja} \left(-F^{-1}_{ak} F^{-1}_{nj} \tau_{ij} + F^{-1}_{aj} \frac{\partial \tau_{ij}}{\partial F_{kn}} \right) F_{ln} \frac{\partial N^B}{\partial x_l} dv_{\mathrm{R}} \\
&= \int_{\mathrm{B}^e} \frac{\partial N^A}{\partial x_j} \left(-\delta_{jk} \tau_{il} + F_{ln} \frac{\partial \tau_{ij}}{\partial F_{kn}} \right) \frac{\partial N^B}{\partial x_l} dv_{\mathrm{R}} \\
&= \int_{\mathcal{B}^e} \frac{\partial N^A}{\partial x_j} \left(-J^{-1} \delta_{jk} \tau_{il} + J^{-1} F_{ln} \frac{\partial \tau_{ij}}{\partial F_{kn}} \right) \frac{\partial N^B}{\partial x_l} dv \\
&= \int_{\mathcal{B}^e} \frac{\partial N^A}{\partial x_j} \left(-J^{-1} \delta_{jk} \tau_{il} + J^{-1} F_{ln} F_{jm} \frac{\partial T_{\mathrm{R},im}}{\partial F_{kn}} + J^{-1} F_{ln} T_{\mathrm{R},im} \delta_{jk} \delta_{mn} \right) \frac{\partial N^B}{\partial x_l} dv \\
&= \int_{\mathcal{B}^e} \frac{\partial N^A}{\partial x_j} \left(-J^{-1} \delta_{jk} \tau_{il} + J^{-1} F_{ln} F_{jm} \frac{\partial T_{\mathrm{R},im}}{\partial F_{kn}} + J^{-1} \delta_{jk} \tau_{il} \right) \frac{\partial N^B}{\partial x_l} dv \\
&= \int_{\mathcal{B}^e} \frac{\partial N^A}{\partial x_j} \left(J^{-1} F_{ln} F_{jm} \frac{\partial T_{\mathrm{R},im}}{\partial F_{kn}} \right) \frac{\partial N^B}{\partial x_l} dv
\end{aligned}$$

or with

$$\mathbb{A}_{ijkl} \stackrel{\text{def}}{=} J^{-1} F_{jm} F_{ln} (\mathbb{A}_{\text{R}})_{imkn}, \qquad \text{with} \qquad \mathbb{A}_{\text{R}} \stackrel{\text{def}}{=} \frac{\partial \mathbf{T}_{\text{R}}}{\partial \mathbf{F}} \tag{3.39}$$

defining a spatial tangent modulus, we have

$$K^{AB}_{u_i u_k} = \int_{\mathcal{B}^e} \frac{\partial N^A}{\partial x_j} \mathbb{A}_{ijkl} \frac{\partial N^B}{\partial x_l} dv. \tag{3.40}$$

3.4 Basic Element Technology

The basic element technology used in this thesis is based of the framework present in [7]. In most cases, when applying the finite element method, the volumetric contribution to the displacement residual is represented in matrix form

$$\mathsf{R}_{\mathbf{u}} = \int_{\mathcal{B}^e} \mathsf{B}^{\top} \mathsf{T} dv, \tag{3.41}$$

where $\mathsf{R}_{\mathbf{u}}$ is the element displacement residual vector, B is the symmetric discrete gradient matrix, and T is the Cauchy stress vector. These three vectors vary depending on whether the problem is plane-strain, axi-symmetric, or three-dimensional. For two dimensions the residual vector, which is returned to ABAQUS as RHS, is

$$\mathsf{R} = \left[R^1_{u_1} R^1_{u_2} R^1_I R^2_{u_1} R^2_{u_2} R^2_I \ldots R^M_{u_1} R^M_{u_2} R^M_I \right]^{\top}, \tag{3.42}$$

and for three dimensions is

$$\mathsf{R} = \left[R^1_{u_1} \; R^1_{u_2} \; R^1_{u_3} \; R^1_I \; R^2_{u_1} \; R^2_{u_2} \; R^2_{u_3} \; R^2_I \; \ldots \; R^M_{u_1} \; R^M_{u_2} \; R^M_{u_3} \; R^M_I \right]^{\top}, \tag{3.43}$$

The matrix form of the tangent matrix is

$$\mathsf{K}_{\mathbf{uu}} = \int_{\mathcal{B}^e} \mathsf{G}^{\top} \mathsf{A} \mathsf{G} \, dv, \tag{3.44}$$

and the global tangent matrix, returned to ABAQUS as AMATRX, is

$$\mathsf{K} = \begin{bmatrix} K^{11}_{u_1u_1} & K^{11}_{u_1u_2} & K^{11}_{u_1I} & K^{12}_{u_1u_1} & K^{12}_{u_1u_2} & K^{12}_{u_1I} & & K^{1M}_{u_1u_1} & K^{1M}_{u_1u_2} & K^{1M}_{u_1I} \\ K^{11}_{u_2u_1} & K^{11}_{u_2u_2} & K^{11}_{u_2I} & K^{12}_{u_2u_1} & K^{12}_{u_2u_2} & K^{12}_{u_2I} & & K^{1M}_{u_2u_1} & K^{1M}_{u_2u_2} & K^{1M}_{u_2I} \\ K^{11}_{Iu_1} & K^{11}_{Iu_2} & K^{11}_{II} & K^{12}_{Iu_1} & K^{12}_{Iu_2} & K^{12}_{II} & & K^{1M}_{Iu_1} & K^{1M}_{Iu_2} & K^{1M}_{II} \\ K^{21}_{u_1u_1} & K^{21}_{u_1u_2} & K^{21}_{u_1I} & K^{22}_{u_1u_1} & K^{22}_{u_1u_2} & K^{22}_{u_1I} & \cdots & K^{2M}_{u_1u_1} & K^{2M}_{u_1u_2} & K^{2M}_{u_1I} \\ K^{21}_{u_2u_1} & K^{21}_{u_2u_2} & K^{21}_{u_2I} & K^{22}_{u_2u_1} & K^{22}_{u_2u_2} & K^{22}_{u_2I} & & K^{2M}_{u_2u_1} & K^{2M}_{u_2u_2} & K^{2M}_{u_2I} \\ K^{21}_{Iu_1} & K^{21}_{Iu_2} & K^{21}_{II} & K^{22}_{Iu_1} & K^{22}_{Iu_2} & K^{22}_{II} & & K^{22}_{Iu_1} & K^{2M}_{\mu u_2} & K^{2M}_{II} \\ & & & \vdots & & & \ddots & & \vdots & \\ K^{M1}_{u_1u_1} & K^{M1}_{u_1u_2} & K^{M1}_{u_1I} & K^{M2}_{u_1u_1} & K^{M2}_{u_1u_2} & K^{M2}_{u_1I} & & K^{MM}_{u_1u_1} & K^{MM}_{u_1u_2} & K^{MM}_{u_1I} \\ K^{M1}_{u_2u_1} & K^{M1}_{u_2u_2} & K^{M1}_{u_2I} & K^{M2}_{u_2u_1} & K^{M2}_{u_2u_2} & K^{M2}_{u_2I} & \cdots & K^{MM}_{u_2u_1} & K^{MM}_{u_2u_2} & K^{MM}_{u_2I} \\ K^{M1}_{Iu_1} & K^{M1}_{Iu_2} & K^{M1}_{II} & K^{M2}_{Iu_1} & K^{M2}_{Iu_2} & K^{M2}_{II} & & K^{MM}_{Iu_1} & K^{MM}_{Iu_2} & K^{MM}_{II} \end{bmatrix} \tag{3.45}$$

To accommodate for both compressible and nearly incompressible material behavior and mitigate *volumetric locking*, we have implemented the so called *F-bar* method [8]. This procedure is based on replacing the deformation gradient suitably such that the incompressibility constraint is enforced as an approximate average throughout the element, rather than point wise at each integration point. The method is based on the distortional-volumetric split of the deformation gradient

$$\mathbf{F} = \mathbf{F}_{\text{dis}}\mathbf{F}_{\text{vol}}\,, \tag{3.46}$$

with

$$\mathbf{F}_{\text{dis}} = J^{-1/3}\mathbf{F}, \quad \mathbf{F}_{\text{vol}} = J^{1/3}\mathbf{1}\,. \tag{3.47}$$

To construct the modified deformation gradient at an integration point of interest, we first determine the deformation gradient at the centroid of the element, denoted by $\mathbf{F}_c$. Then the modified deformation gradient is constructed as

$$\bar{\mathbf{F}} = \left(\frac{\det \mathbf{F}_c}{\det \mathbf{F}}\right)^{1/3} \mathbf{F}. \tag{3.48}$$

When stresses are computed at the integration points, the modified deformation gradient $\bar{\mathbf{F}}$ is used in place of $\mathbf{F}$. This ensures that all of the integration points withing the element share the same total volumetric deformation gradient, specifically $\det \mathbf{F}_c$. This formulation does not change the computation of the residual (3.37) at the integration point, simply that $\bar{\mathbf{F}}$ is used to compute the constitutive response, rather than $\mathbf{F}$. However, the tangent computation (3.40) must be modified to

$$\mathsf{K}_{\mathbf{uu}} = \underbrace{\int_{\mathcal{B}^e} \mathsf{G}^{\top} \mathsf{A} \mathsf{G} \, dv}_{\text{standard terms}} + \underbrace{\int_{\mathcal{B}^e} \mathsf{G}^{\top} \mathsf{Q} (\mathsf{G}_0 - \mathsf{G}) \, dv}_{\text{additional terms}} , \tag{3.49}$$

with

$$\mathbb{Q} = \frac{1}{3} \mathbb{A} : (\mathbf{1} \otimes \mathbf{1}) - \frac{2}{3} \mathbf{T} \otimes \mathbf{1} . \tag{3.50}$$

3.4.1 Plane Strain Problem

For plane strain elements, as mentioned before, have the condition that $F_{33} = 1$, and $F_{13} = F_{31} = F_{23} = F_{32} = 0$; and the stress vector T is given by

$$\mathsf{T} = [T_{11} \; T_{22} \; T_{12}]^{\top} . \tag{3.51}$$

In order to ensure a nearly incompressible material behavior the *F-Bar* method [8] will be employed and for plane strain this reduces to

$$\begin{bmatrix} \bar{F}_{11} & \bar{F}_{12} & 0 \\ \bar{F}_{21} & \bar{F}_{22} & 0 \\ 0 & 0 & 1 \end{bmatrix} = \left(\frac{F_{c,11} F_{c,22} - F_{c,12} F_{c,21}}{F_{11} F_{22} - F_{12} F_{21}} \right)^{1/2} \begin{bmatrix} F_{11} & F_{12} & 0 \\ F_{21} & F_{22} & 0 \\ 0 & 0 & 1 \end{bmatrix} , \tag{3.52}$$

with $F_{c,ij}$ the deformation gradient at the centroid of the element. Correspondingly, in plane-strain, the tangent modification (3.49) is now given by

$$\mathbb{Q} = \frac{1}{2} \mathbb{A} : (\mathbf{1} \otimes \mathbf{1}) - \frac{1}{2} \mathbf{T} \otimes \mathbf{1} \tag{3.53}$$

where

$$[\mathbb{A}\colon(\mathbf{1}\otimes\mathbf{1})] = \begin{bmatrix} A_{11}+A_{14} & 0 & 0 & 0 & A_{11}+A_{14} \\ A_{21}+A_{24} & 0 & 0 & 0 & A_{21}+A_{24} \\ A_{31}+A_{34} & 0 & 0 & 0 & A_{31}+A_{34} \\ A_{41}+A_{44} & 0 & 0 & 0 & A_{41}+A_{44} \end{bmatrix} \tag{3.54}$$

with

$$\mathsf{A}_{mn} = \mathbb{A}_{ijkl}$$

denoting the matrix representation of $\mathbb{A}$ using the following transformation table

m/n	i/k	j/l
1	1	1
2	2	1
3	1	2
4	2	2

and with

$$[\mathbf{T}\otimes\mathbf{1}] = \begin{bmatrix} T_{11} & 0 & 0 & 0 & T_{11} \\ T_{21} & 0 & 0 & 0 & T_{21} \\ T_{12} & 0 & 0 & 0 & T_{12} \\ T_{22} & 0 & 0 & 0 & T_{22} \end{bmatrix} \tag{3.55}$$

for the plane strain formulation.

3.4.2 Axisymmetric Problem

As mentioned earlier, for an axisymmetric element we have the condition that $F_{13} = F_{31} = F_{23} = F_{32} = 0$, and $F_{33} = R/R_0$, also the stress vector T is given by

$$\mathsf{T} = [T_{11}\ T_{22}\ T_{12}\ T_{33}]^{\top}\ . \tag{3.56}$$

Once again the *F-Bar* method [8] will be employed to prevent volumetric locking and for the axisymmetric case the method takes the form

$$\bar{\mathbf{F}} = \left(\frac{\det \mathbf{F}_c}{\det \mathbf{F}}\right)^{1/3} \mathbf{F}\,, \tag{3.57}$$

where both F_{33} and F_{c33} are computed before applying the F-bar method. The tangents need to be corrected according to (3.49) with

$$[\mathbb{A} : (\mathbf{1} \otimes \mathbf{1})] = \begin{bmatrix} A_{11}+A_{14}+A_{15} & 0 & 0 & A_{11}+A_{14}+A_{15} & A_{11}+A_{14}+A_{15} \\ A_{21}+A_{24}+A_{25} & 0 & 0 & A_{21}+A_{24}+A_{25} & A_{21}+A_{24}+A_{25} \\ A_{31}+A_{34}+A_{35} & 0 & 0 & A_{31}+A_{34}+A_{35} & A_{31}+A_{34}+A_{35} \\ A_{41}+A_{44}+A_{45} & 0 & 0 & A_{41}+A_{44}+A_{45} & A_{41}+A_{44}+A_{45} \\ A_{51}+A_{54}+A_{55} & 0 & 0 & A_{51}+A_{54}+A_{55} & A_{51}+A_{54}+A_{55} \end{bmatrix} \tag{3.58}$$

where

$$\mathsf{A}_{mn} = \mathbb{A}_{ijkl}$$

using the following transformation table

m/n	i/k	j/l
1	1	1
2	2	1
3	1	2
4	2	2
5	3	3

and with

$$[\mathbf{T} \otimes \mathbf{1}] = \begin{bmatrix} T_{11} & 0 & 0 & T_{11} & T_{11} \\ T_{21} & 0 & 0 & T_{21} & T_{21} \\ T_{12} & 0 & 0 & T_{12} & T_{12} \\ T_{22} & 0 & 0 & T_{22} & T_{22} \\ T_{33} & 0 & 0 & T_{33} & T_{33} \end{bmatrix} \tag{3.59}$$

for the axisymmetric formulation.

3.4.3 Three Dimensional Problem

Finally the three dimensional form of the *F-Bar* method [8] will be presented. For the three-dimensional 8-node linear brick element developed the node ordering in the natural coordinates is shown in Fig. 4.1. The stress vector T now takes on the form

$$\mathsf{T} = [T_{11}\ T_{22}\ T_{33}\ T_{12}\ T_{23}\ T_{13}]^{\top}\ . \tag{3.60}$$

and again

$$\bar{\mathbf{F}} = \left(\frac{\det \mathbf{F}_c}{\det \mathbf{F}}\right)^{1/3} \mathbf{F}\,, \tag{3.61}$$

The tangents need to be corrected according to (3.49) with

$$[\mathbb{A}\colon(\mathbf{1}\otimes\mathbf{1})] = \begin{bmatrix} A_{11}+A_{15}+A_{19} & 0 & 0 & 0 & A_{11}+A_{15}+A_{19} & 0 & 0 & 0 & A_{11}+A_{15}+A_{19} \\ A_{21}+A_{25}+A_{29} & 0 & 0 & 0 & A_{21}+A_{25}+A_{29} & 0 & 0 & 0 & A_{21}+A_{25}+A_{29} \\ A_{31}+A_{35}+A_{39} & 0 & 0 & 0 & A_{31}+A_{35}+A_{39} & 0 & 0 & 0 & A_{31}+A_{35}+A_{39} \\ A_{41}+A_{45}+A_{49} & 0 & 0 & 0 & A_{41}+A_{45}+A_{49} & 0 & 0 & 0 & A_{41}+A_{45}+A_{49} \\ A_{51}+A_{55}+A_{59} & 0 & 0 & 0 & A_{51}+A_{55}+A_{59} & 0 & 0 & 0 & A_{51}+A_{55}+A_{59} \\ A_{61}+A_{65}+A_{69} & 0 & 0 & 0 & A_{61}+A_{65}+A_{69} & 0 & 0 & 0 & A_{61}+A_{65}+A_{69} \\ A_{71}+A_{75}+A_{79} & 0 & 0 & 0 & A_{71}+A_{75}+A_{79} & 0 & 0 & 0 & A_{71}+A_{75}+A_{79} \\ A_{81}+A_{85}+A_{89} & 0 & 0 & 0 & A_{81}+A_{85}+A_{89} & 0 & 0 & 0 & A_{81}+A_{85}+A_{89} \\ A_{91}+A_{95}+A_{99} & 0 & 0 & 0 & A_{91}+A_{95}+A_{99} & 0 & 0 & 0 & A_{91}+A_{95}+A_{99} \end{bmatrix} \tag{3.62}$$

where

$$\mathsf{A}_{mn} = \mathbb{A}_{ijkl}$$

using the following transformation table

m/n	i/k	j/l
1	1	1
2	2	1
3	3	1
4	1	2
5	2	2
6	3	2
7	1	3
8	2	3
9	3	3

and with

$$[\mathbf{T} \otimes \mathbf{1}] = \begin{bmatrix} T_{11} & 0 & 0 & 0 & T_{11} & 0 & 0 & 0 & T_{11} \\ T_{21} & 0 & 0 & 0 & T_{21} & 0 & 0 & 0 & T_{21} \\ T_{31} & 0 & 0 & 0 & T_{31} & 0 & 0 & 0 & T_{31} \\ T_{12} & 0 & 0 & 0 & T_{12} & 0 & 0 & 0 & T_{12} \\ T_{22} & 0 & 0 & 0 & T_{22} & 0 & 0 & 0 & T_{22} \\ T_{32} & 0 & 0 & 0 & T_{32} & 0 & 0 & 0 & T_{32} \\ T_{13} & 0 & 0 & 0 & T_{13} & 0 & 0 & 0 & T_{13} \\ T_{23} & 0 & 0 & 0 & T_{23} & 0 & 0 & 0 & T_{23} \\ T_{33} & 0 & 0 & 0 & T_{33} & 0 & 0 & 0 & T_{33} \end{bmatrix} \tag{3.63}$$

for the three-dimensional formulation.

CHAPTER 4

DISCRETIZATION USING ISO-PARAMETRIC LAGRANGIAN SHAPE FUNCTIONS

This chapter presents the standard techniques for the discretization of an arbitrary geometry using isoparametric shape functions. Finite Elements will be employed in three different cases. These are plain-strain, axi-symmetric, and three dimensional. Plain-strain assumes no strain in one of the three directions, axi-symmetric assumes that the geometry has some radial symmetry present, and the three dimensional shape functions are used for an arbitrary three dimensional shape. The distinction is made between the first two types and the general three-dimensional type due to the increased amount of computational time necessary for the full 3D problem. If a symmetry exists within the problem then the user can simply choose the appropriate element for the problem in order to save themselves computational expense if the geometry exhibits some symmetry such as a block or a cylinder. For a more detailed discussion of finite element shape functions consult [27] and [12].

4.1 Two-Dimensional Elements

For the two-dimensional elements developed, the node ordering in the natural coordinates is shown in Figure 4.1. Referring to Figure 4.1, the shape functions for the 4-node linear element with respect to the natural coordinates are given by

$$\begin{aligned} N^1 &= \frac{1}{4}(1-\xi)(1-\eta) \\ N^2 &= \frac{1}{4}(1+\xi)(1-\eta) \\ N^3 &= \frac{1}{4}(1+\xi)(1+\eta) \\ N^4 &= \frac{1}{4}(1-\xi)(1+\eta). \end{aligned}$$

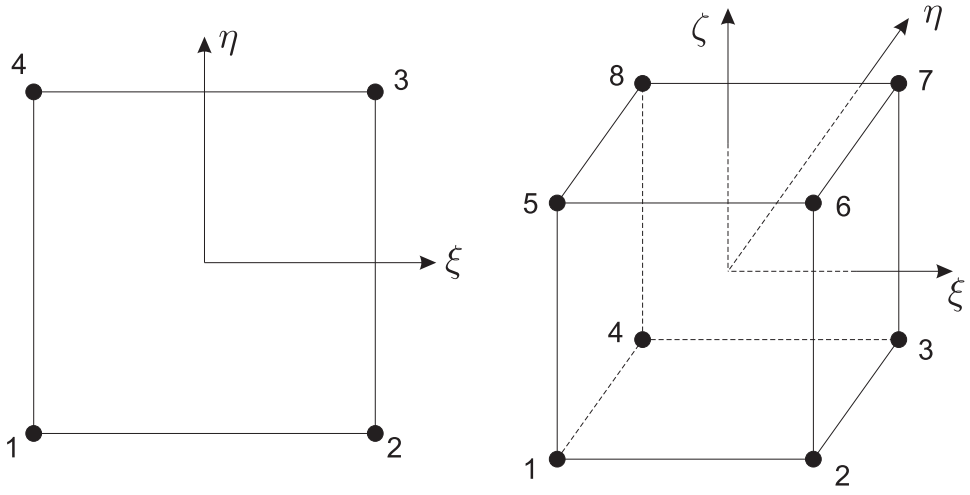

Figure 4.1 Two-dimensional linear quadrilateral, and three-dimensional linear brick isoparametric master elements, with the node numbering as shown.

4.1.1 Planar Elements

For a plane-strain element we have the condition that $F_{33} = 1$, and $F_{13} = F_{31} = F_{23} = F_{32} = 0$. Furthermore, the B-matrix, also known as the symmetric discrete gradient matrix, is given by

$$\mathsf{B} = \begin{bmatrix} \dfrac{\partial N^1}{\partial x_1} & 0 & \dfrac{\partial N^2}{\partial x_1} & 0 & \cdots & \dfrac{\partial N^M}{\partial x_1} & 0 \\ 0 & \dfrac{\partial N^1}{\partial x_2} & 0 & \dfrac{\partial N^2}{\partial x_2} & \cdots & 0 & \dfrac{\partial N^M}{\partial x_2} \\ \dfrac{\partial N^1}{\partial x_2} & \dfrac{\partial N^1}{\partial x_1} & \dfrac{\partial N^2}{\partial x_2} & \dfrac{\partial N^2}{\partial x_1} & \cdots & \dfrac{\partial N^M}{\partial x_2} & \dfrac{\partial N^M}{\partial x_1} \end{bmatrix} \tag{4.1}$$

where M is the total number of nodes in the element. The last matrix necessary for discretization is the so called non-symmetric discrete gradient matrix G given by

$$\mathsf{G} = \begin{bmatrix} \dfrac{\partial N^1}{\partial x_1} & 0 & \dfrac{\partial N^2}{\partial x_1} & 0 & \cdots & \dfrac{\partial N^M}{\partial x_1} & 0 \\ 0 & \dfrac{\partial N^1}{\partial x_1} & 0 & \dfrac{\partial N^2}{\partial x_1} & \cdots & 0 & \dfrac{\partial N^M}{\partial x_1} \\ \dfrac{\partial N^1}{\partial x_2} & 0 & \dfrac{\partial N^2}{\partial x_2} & 0 & \cdots & \dfrac{\partial N^M}{\partial x_2} & 0 \\ 0 & \dfrac{\partial N^1}{\partial x_2} & 0 & \dfrac{\partial N^2}{\partial x_2} & \cdots & 0 & \dfrac{\partial N^M}{\partial x_2} \end{bmatrix} \tag{4.2}$$

4.1.2 Axisymmetric Elements

The axisymmetric problem is also modeled as 2D geometry with some differences however. For an axisymmetric element we have the condition that $F_{13} = F_{31} = F_{23} = F_{32} = 0$, and $F_{33} = R/R_0$. The integration is modified such that $\int_{\mathcal{B}_t^e} dxdy \to \int_{\mathcal{B}_t^e} 2\pi r dr dz$. In the numerical implementation F_{33} is computed as R/R_0, and numerically this is accomplished by

$$R = \sum N^A x_1^A \,, \tag{4.3}$$

$$R_0 = \sum N^A X_1^A \,, \tag{4.4}$$

where x_1^A are the current 1-coordinates of the nodes, and X_1^A are the reference 1-coordinates of the nodes. Note that this scheme automatically implies that our axisymmetric element formulation assumes the radial direction is the 1-direction. The B-matrix is given by

$$\mathsf{B} = \begin{bmatrix} \dfrac{\partial N^1}{\partial x_1} & 0 & \dfrac{\partial N^2}{\partial x_1} & 0 & \cdots & \dfrac{\partial N^M}{\partial x_1} & 0 \\ 0 & \dfrac{\partial N^1}{\partial x_2} & 0 & \dfrac{\partial N^2}{\partial x_2} & \cdots & 0 & \dfrac{\partial N^M}{\partial x_2} \\ \dfrac{\partial N^1}{\partial x_2} & \dfrac{\partial N^1}{\partial x_1} & \dfrac{\partial N^2}{\partial x_2} & \dfrac{\partial N^2}{\partial x_1} & \cdots & \dfrac{\partial N^M}{\partial x_2} & \dfrac{\partial N^M}{\partial x_1} \\ \dfrac{N^1}{R} & 0 & \dfrac{N^2}{R} & 0 & \cdots & \dfrac{N^M}{R} & 0 \end{bmatrix} \tag{4.5}$$

Finally, the standard non-symmetric discrete gradient matrix in (3.49) is given by

$$\mathsf{G} = \begin{bmatrix} \dfrac{\partial N^1}{\partial x_1} & 0 & \dfrac{\partial N^2}{\partial x_1} & 0 & \cdots & \dfrac{\partial N^M}{\partial x_1} & 0 \\ 0 & \dfrac{\partial N^1}{\partial x_1} & 0 & \dfrac{\partial N^2}{\partial x_1} & \cdots & 0 & \dfrac{\partial N^M}{\partial x_1} \\ \dfrac{\partial N^1}{\partial x_2} & 0 & \dfrac{\partial N^2}{\partial x_2} & 0 & \cdots & \dfrac{\partial N^M}{\partial x_2} & 0 \\ 0 & \dfrac{\partial N^1}{\partial x_2} & 0 & \dfrac{\partial N^2}{\partial x_2} & \cdots & 0 & \dfrac{\partial N^M}{\partial x_2} \\ \dfrac{N^1}{R} & 0 & \dfrac{N^2}{R} & 0 & \cdots & \dfrac{N^M}{R} & 0 \end{bmatrix} \tag{4.6}$$

the above matrices are used to write element subroutines in order to carry out the numerical procedures.

4.1.3 Three Dimensional Elements

For the three-dimensional 8-node linear brick element developed the node ordering in the natural coordinates is shown in Figure 4.1. Referring to Figure 4.1, the shape functions for the 8-node linear brick element with respect to the natural coordinates are given by

$$
\begin{aligned}
N^1 &= \frac{1}{8}(1-\xi)(1-\eta)(1-\zeta), \quad N^2 = \frac{1}{8}(1+\xi)(1-\eta)(1-\zeta),\\
N^3 &= \frac{1}{8}(1+\xi)(1+\eta)(1-\zeta), \quad N^4 = \frac{1}{8}(1-\xi)(1+\eta)(1-\zeta),\\
N^5 &= \frac{1}{8}(1-\xi)(1-\eta)(1+\zeta), \quad N^6 = \frac{1}{8}(1+\xi)(1-\eta)(1+\zeta),\\
N^7 &= \frac{1}{8}(1+\xi)(1+\eta)(1+\zeta), \quad N^8 = \frac{1}{8}(1-\xi)(1+\eta)(1+\zeta).
\end{aligned}
$$

Here the B-matrix is given by

$$
\mathsf{B} = \begin{bmatrix}
\dfrac{\partial N^1}{\partial x_1} & 0 & 0 & \dfrac{\partial N^2}{\partial x_1} & 0 & 0 & \cdots & \dfrac{\partial N^M}{\partial x_1} & 0 & 0 \\
0 & \dfrac{\partial N^1}{\partial x_2} & 0 & 0 & \dfrac{\partial N^2}{\partial x_2} & 0 & \cdots & 0 & \dfrac{\partial N^M}{\partial x_2} & 0 \\
0 & 0 & \dfrac{\partial N^1}{\partial x_3} & 0 & 0 & \dfrac{\partial N^2}{\partial x_3} & \cdots & 0 & 0 & \dfrac{\partial N^M}{\partial x_3} \\
\dfrac{\partial N^1}{\partial x_2} & \dfrac{\partial N^1}{\partial x_1} & 0 & \dfrac{\partial N^2}{\partial x_2} & \dfrac{\partial N^2}{\partial x_1} & 0 & \cdots & \dfrac{\partial N^M}{\partial x_2} & \dfrac{\partial N^M}{\partial x_1} & 0 \\
0 & \dfrac{\partial N^1}{\partial x_3} & \dfrac{\partial N^1}{\partial x_2} & 0 & \dfrac{\partial N^2}{\partial x_3} & \dfrac{\partial N^2}{\partial x_2} & \cdots & 0 & \dfrac{\partial N^M}{\partial x_3} & \dfrac{\partial N^M}{\partial x_2} \\
\dfrac{\partial N^1}{\partial x_3} & 0 & \dfrac{\partial N^1}{\partial x_1} & \dfrac{\partial N^2}{\partial x_3} & 0 & \dfrac{\partial N^2}{\partial x_1} & \cdots & \dfrac{\partial N^M}{\partial x_3} & 0 & \dfrac{\partial N^M}{\partial x_1}
\end{bmatrix} \tag{4.7}
$$

where again M is the total number of nodes in the element. Finally the non-symmetric discrete gradient matrix for a three-dimensional brick element is given as

$$\mathsf{G} = \begin{bmatrix} \frac{\partial N^1}{\partial x_1} & 0 & 0 & \frac{\partial N^2}{\partial x_1} & 0 & 0 & \cdots & \frac{\partial N^M}{\partial x_1} & 0 & 0 \\ 0 & \frac{\partial N^1}{\partial x_1} & 0 & 0 & \frac{\partial N^2}{\partial x_1} & 0 & \cdots & 0 & \frac{\partial N^M}{\partial x_1} & 0 \\ 0 & 0 & \frac{\partial N^1}{\partial x_1} & 0 & 0 & \frac{\partial N^2}{\partial x_1} & \cdots & 0 & 0 & \frac{\partial N^M}{\partial x_1} \\ \frac{\partial N^1}{\partial x_2} & 0 & 0 & \frac{\partial N^2}{\partial x_2} & 0 & 0 & \cdots & \frac{\partial N^M}{\partial x_2} & 0 & 0 \\ 0 & \frac{\partial N^1}{\partial x_2} & 0 & 0 & \frac{\partial N^2}{\partial x_2} & 0 & \cdots & 0 & \frac{\partial N^M}{\partial x_2} & 0 \\ 0 & 0 & \frac{\partial N^1}{\partial x_2} & 0 & 0 & \frac{\partial N^2}{\partial x_2} & \cdots & 0 & 0 & \frac{\partial N^M}{\partial x_2} \\ \frac{\partial N^1}{\partial x_3} & 0 & 0 & \frac{\partial N^2}{\partial x_3} & 0 & 0 & \cdots & \frac{\partial N^M}{\partial x_3} & 0 & 0 \\ 0 & \frac{\partial N^1}{\partial x_3} & 0 & 0 & \frac{\partial N^2}{\partial x_3} & 0 & \cdots & 0 & \frac{\partial N^M}{\partial x_3} & 0 \\ 0 & 0 & \frac{\partial N^1}{\partial x_3} & 0 & 0 & \frac{\partial N^2}{\partial x_3} & \cdots & 0 & 0 & \frac{\partial N^M}{\partial x_3} \end{bmatrix} \tag{4.8}$$

CHAPTER 5

VERIFICATION OF THE FINITE ELEMENT FORMULATION

The first formal result achieved was the verification of the possibility of a non-linear finite element implementation of the Beer-Lambert law. This result motivated the extension of the numerical method to two and eventually three dimensions with weak coupling to a large deformation theory.

The possibility of a fully functional LASMP FEM is not possible without the above precursors. Once these results were obtained a simple homogeneous (equal value of light intensity throughout) SMP effect driven by whether or not the light intensity was above a critical value, $I \geq I_c$. The assumption of homogeneity is reasonably valid for optically thin materials, however for optically thick material the light intensity may vary greatly from one region to another which will cause inhomogeneity in the constitutive response.

5.1 One-Dimensional Verification of the SUPG Formulation

As an initial step toward the fully coupled three-dimensional theory of light and deformation, the Beer-Lambert law will first be numerically verified using a simple one-dimensional finite element implementation with the aid of MATLAB. The strong form for this simplified one-dimensional case takes the form

$$\text{1-D Beer-Lambert Law} \begin{cases} d\dfrac{dI}{dx} + \sigma I = 0 \quad \text{in } \mathcal{B}_t \\ \\ I = \breve{I} \quad \text{on } \mathcal{S}_- \end{cases} \tag{5.1}$$

and note that $d = \pm 1$ due to the one-dimensional nature of the problem. Here it will be assumed that $d = 1$ for simplicity. The one-dimensional residual and tangent matrix are therefore

$$R_I^A = \int_{\mathcal{B}_t^e} N^A \left(\frac{dI}{dx} + \sigma I \right) dx + \int_{\mathcal{B}_t^e} \tau \frac{dN^A}{dx} \left(\frac{dI}{dx} + \sigma I \right) dx, \tag{5.2}$$

and

$$K_{II}^{AB} = -\int_{\mathcal{B}_t^e} N^A \left(\frac{\partial N^B}{\partial x} + \frac{\partial \sigma}{\partial I} N^B I + \sigma N^B \right) dx \\ - \int_{\mathcal{B}_t^e} \tau \frac{\partial N^A}{\partial x} \left(\frac{\partial N^B}{\partial x} + \frac{\partial \sigma}{\partial I} N^B I + \sigma N^B \right) dx. \tag{5.3}$$

These simplified forms are implemented in MATLAB, and the code is provided in the Appendix. In order to verify this formulation a simple analytical example will compared to the simulation results. This scenario will involve constant light absorptivity so the governing equation can be solved analytically

$$\begin{aligned} \frac{dI}{dx} + \sigma I &= 0, \\ \frac{dI}{dx} &= -\sigma I, \\ \frac{dI}{I} &= -\sigma dx, \end{aligned}$$

and integration over the body $\mathcal{B}_t$ gives

$$\begin{aligned} \int_{\mathcal{B}_t} \frac{dI}{I} &= \int_{\mathcal{B}_t} \sigma dx, \\ \ln(I) &= -\sigma x + C, \end{aligned}$$

or in other words,

$$I = I_0 e^{-\sigma x} \tag{5.4}$$

which is the analytic solution and is compared against the finite element method in Figure 5.1. The case of light absorptivity which depends on the value of the light intensity is also compared against the finite element method in Figure 5.2.

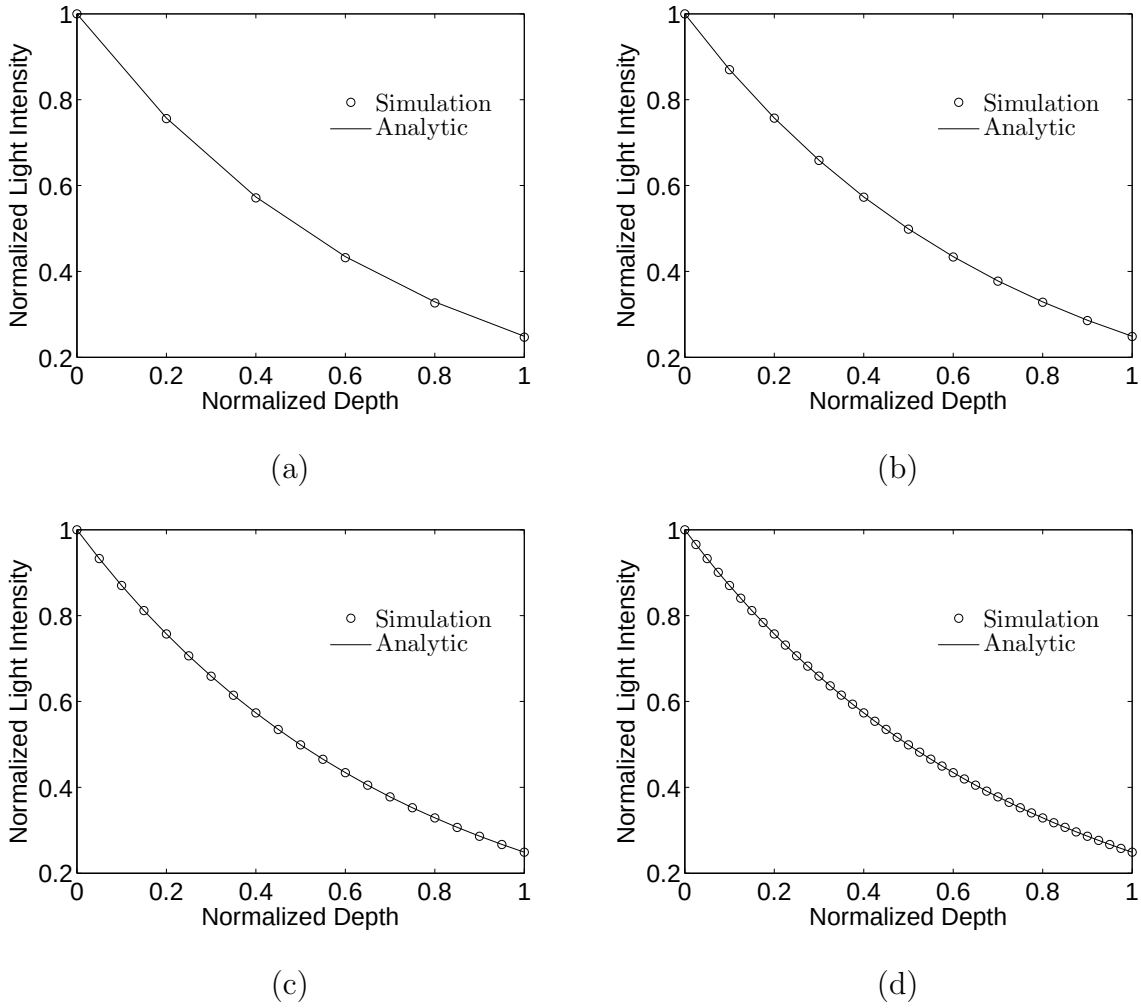

Figure 5.1 One-dimensional verification with $\sigma = 13,900\,\mathrm{cm}^{-1}$. The analytical solution is $I = I_0 e^{-\sigma x}$ i.e. $I = I_0 e^{-13{,}900x}$ and is compared against the numerical solution using (a) 5 elements, (b) 10 elements, (c) 20 elements and (d) 40 elements.

Note that the normalized depth is the coordinate position divided by the length of the member, i.e. $\frac{x}{l}$ and the normalized light intensity is $\frac{I}{I_0}$

5.2 Two- and Three-dimensional Verification of the Beer-Lambert Problem

This section will showcase the verification of the strong form with no deformation, so only light will be present in the simulations to follow. The simplest possible problem,

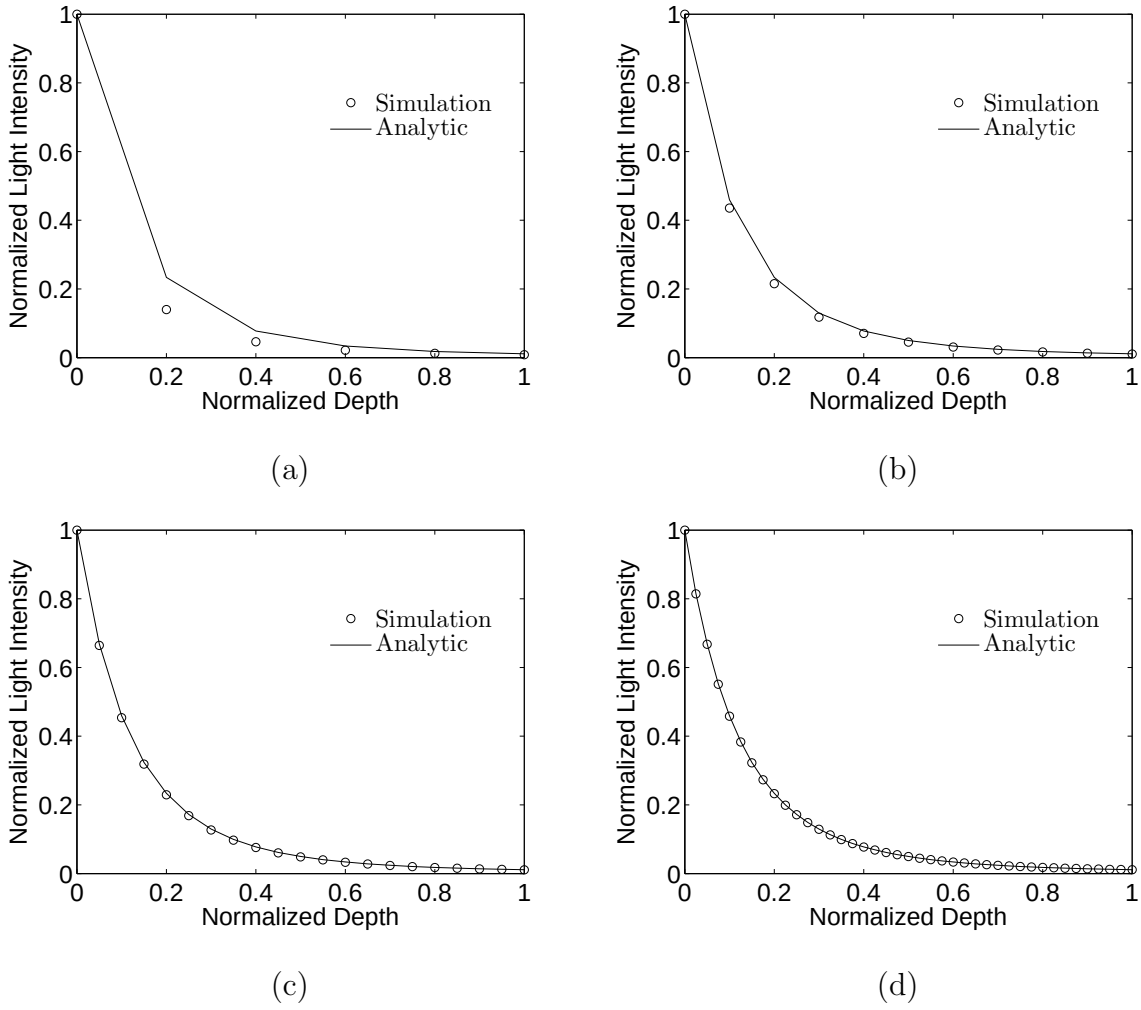

Figure 5.2 One-dimensional verification with $\sigma = 13,900 \ln I \, \mathrm{cm}^{-1}$. The analytical solution is $I = e^{\ln I_0 e^{-\sigma x}}$ i.e. $I = e^{I_0 e^{-13,900x}}$ and is compared against the numerical solution using (a) 5 elements, (b) 10 elements, (c) 20 elements and (d) 40 elements.

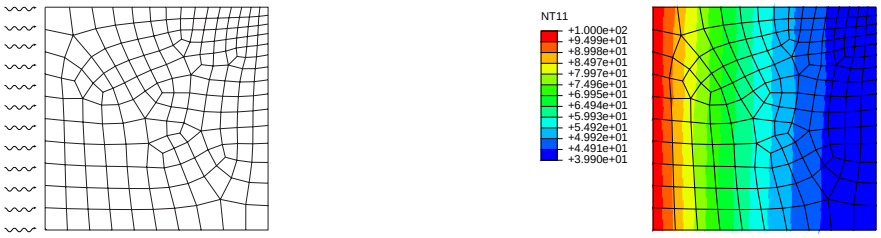

a) b)

Figure 5.3 (a) Mesh and boundary conditions of a plane-strain simulation. (b) Contour plot of light intensity.

light traveling strictly in one direction incident perpendicular to a rectangular face, will be verified for the UPE4, UAX4, and U3D8 element types.

Consider now the strong form (3.13) with $\mathbf{d} = \begin{pmatrix} 1 & 0 & 0 \end{pmatrix}^\top$, i.e. light is traveling in the positive x-direction. Due to the definition of the boundaries for Equation (3.13) light will only be incident upon the left face of the rectangle and this reduces the strong form to

$$\begin{cases} \dfrac{dI}{dx_1} I + \sigma I = 0 \text{ in } \mathcal{B}_t \\ \\ \qquad\qquad I = I_0, \text{ on } \mathcal{S}_- \end{cases} \tag{5.5}$$

which is the same form presented in the section on one-dimensional verification. Therefore the analytic solution for constant absorptivity will take the form of a decreasing exponential. The results of the ABAQUS simulation shown in Figure 5.3 is compared against the analytic solution in Figure 5.5. These results show that our element technology has a significant amount of error due to the numerical diffusion and zero flux boundary condition. Future work will be aimed at improving these error bounds.

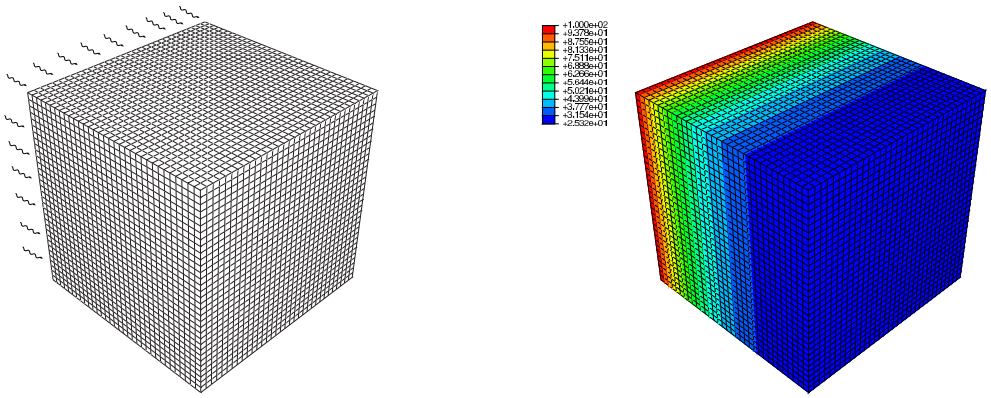

a) b)

Figure 5.4 (a) Mesh and boundary conditions of a three-dimensional simulation. (b) Contour plot of light intensity.

5.3 Verification of the Large Deformation Problem

In the absence of light the theory reduces to a typical hyperelastic neo-Hookean material. The Cauchy stress then takes the form

$$\mathbf{T} = \mu \left(\mathbf{B}_{\text{dis}}\right)_0 + K(\ln J)\mathbf{1} \tag{5.6}$$

To approximate a nearly incompressible neo-Hookean material we take $K = 10^3\mu$. This form of the constitutive equation will be used to verify the UEL against simple analytical solutions. The analytical solutions will make a further assumption that the material is completely incompressible, i.e. $J = 1$. The Cauchy stress under this assumption now takes the form

$$\mathbf{T} = -p\mathbf{1} + \mu\mathbf{B} \tag{5.7}$$

where p is a constitutively indeterminate pressure. For simple plane-strain compression in the x_1 direction the analytical solution for the stretch-stress behavior is

$$T_{11} = \mu\left(\lambda^2 - \lambda^{-2}\right) \tag{5.8}$$

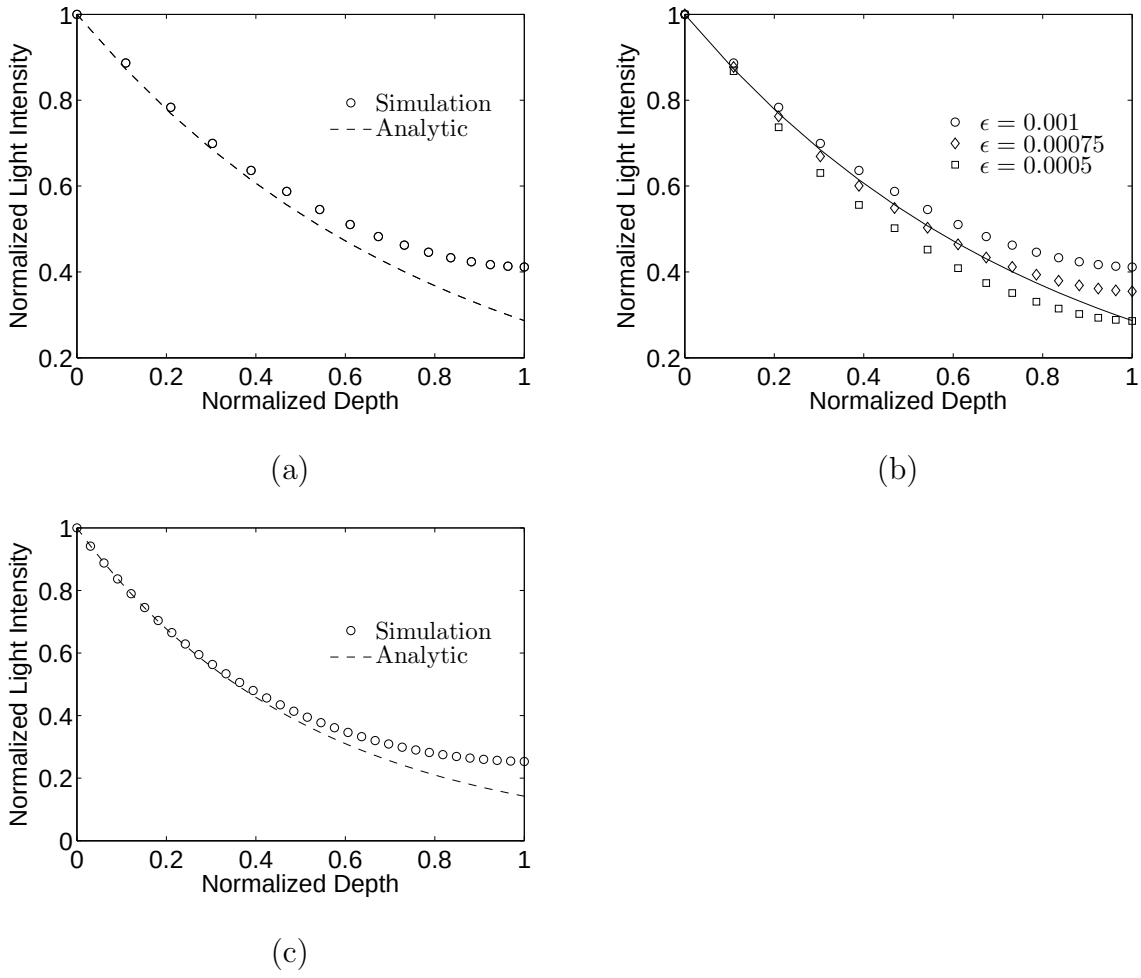

Figure 5.5 (a) Comparison of plane-strain simulation to the analytic solution. (b) A parametric study showing the result of varying the numerical diffusivity in a plane-strain simulation. (c) Comparison of 3D simulation to analytic solution.

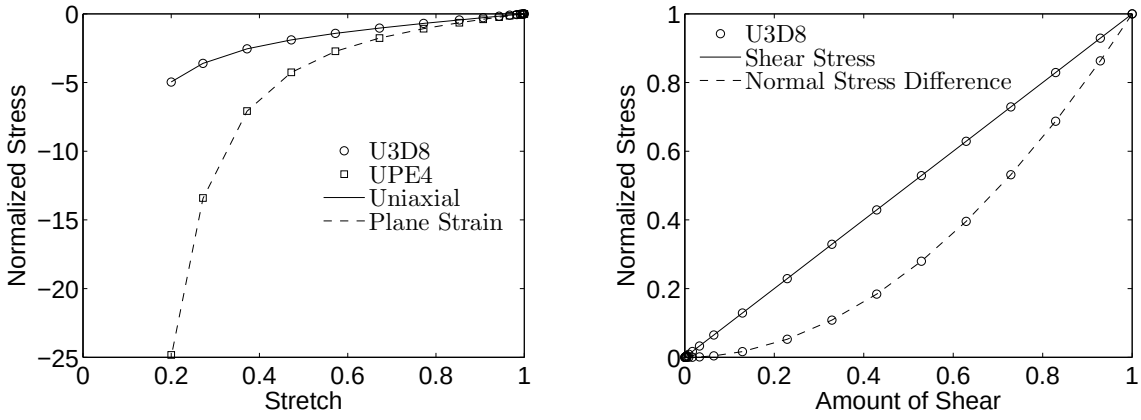

(a) (b)

Figure 5.6 Comparison of numerical solutions against analytical solution for the deformation problem only: (a) normalized stress T_{11}/G versus stretch λ behavior in simple compression. (b) Normalized stress T_{12}/G versus amount of shear γ in shear.

which will be compared against the result computed by using a single UPE4 element, see Figure 5.6. These results will also be compared against simple uniaxial compression results obtained by a single U3D8 element, see Figure 5.6. The stretch-stress behavior for uniaxial compression is given by

$$T_{11} = \mu \left(\lambda^2 - \lambda^{-1} \right). \tag{5.9}$$

The numerical response of a single U3D8 element to simple shear will be compared next to the analytical result, see Figure 5.6. The analytic response to simple shear is

$$T_{12} = \mu\gamma \tag{5.10}$$

and the normal stress difference is

$$T_{11} - T_{33} = \mu\gamma^2 \tag{5.11}$$

where again μ is the shear modulus and γ is the amount of shear. These results verify our element technology when dealing with large mechanical deformations in the absence of light.

CHAPTER 6

NUMERICAL EXAMPLE

This chapter showcases a simple LASMP loading and unloading cycle, see Figure 6.1(a). The geometry in question is made of two sections, the top section is modeled as an incompressible rubber like material which has no response to light, and the bottom section is a light active PMC material. The geometry is meshed with 520 elements and the simulation is carried out under the assumption of plane strain. For simplicity the bulk and shear modulus of the rubber and the first and second network of the PMC will be identical. Listed below are the material parameters which were used.

Table 6.1 Material parameters used for the LASMP cycle simulation.

Parameter	Value
μ	1.0×10^6 MPa
K	1.0×10^9 MPa
σ	5.0×10^3 cm^{-1}
α_{UB}	118 $\text{Lmol}^{-1}\text{cm}^{-1}$
α_B	118 $\text{Lmol}^{-1}\text{cm}^{-1}$
C_0	0.75 molL^{-1}
I_0	100.0, mWcm^{-2}
ν	1.0×10^{14} Hz

The cycle has four phases to it. The first is simple compression by a rigid surface, see Figure 6.1(c). After deformation the body is held and irradiated with light which initiates the formation of the second network. During irradiation the PMC is now in a newly formed stress free configuration, the rubber is not however. This causes the

PMC to absorb some of the stress within the rubber, see Figure 6.1(d). After some time the rigid surface is released. At this point the PMC is in its remembered shape and the rubber has unloaded. The PMC will hold this shape until irradiated with a new frequency of light below the critical frequency ν_{cr}. The last and final phase is the irradiation of the body with a frequency below ν_{cr} which will initiate the reverse reaction within the PMC, see Figure 6.1(e). After enough time the reverse reaction will complete and the body will return to its initial configuration, Figure 6.1(f).

This simulation showcases the potential for the design of products which incorporate LASMPs with other materials which are already utilized in industry. Materials which do not respond to photo-loading can be used as a backbone for light activated polymers to design more complex shape recovery processes.

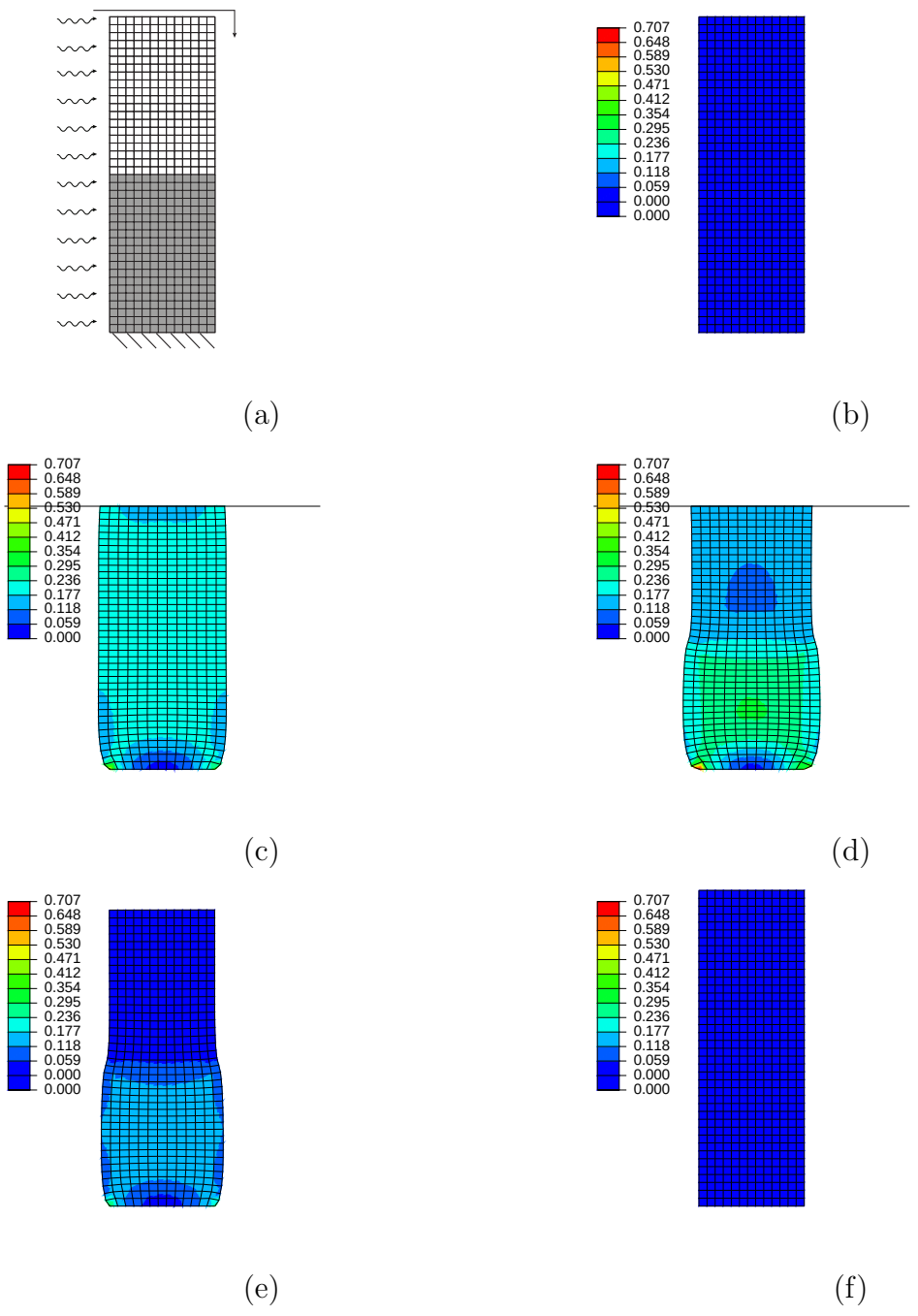

Figure 6.1 Cycle of LASMP loading and unloading (all contour plots display the logarithmic strain): (a) Mesh and BCs. (b) Initial configuration. (c) Simple compression. (d) Body held and irradiated. (e) Body released. (f) Return to initial configuration.

CHAPTER 7

CONCLUSION AND FUTURE WORK

In conclusion a coupled finite element method for light activated polymers has been developed. The FEM has been implemented and verified as an implicit Newton-Raphson scheme in the commercial software package ABAQUS standard as a user defined subroutine for plane strain, axisymmetric, and three dimensional geometries. Neo-hookean constitutive relations were utilized to carry out simulations for both homogeneous and inhomogeneous formation of the second polymer network. Simulations were also carried out for a specific light activated polymer, PMC, which utilized a photochemical reaction rate which drove the formation of the new network.

In future work, the errors present in the light intensity solutions will need to be improved through further research and development of more robust and sophisticated numerical methods. This work can be used as a foundation for the development of other user defined subroutines for different classes of light activated polymers by changing the reaction rate. Similarly an extension of the method to polymers which exhibit more than two networks can be carried out.

Other than improvement of the numerical method itself experimental verification will need to be performed in order to validate the method. This will require the design of experimental setups which utilize photo, chemical, and mechanical apparatuses. Research into more complex constitutive responses of the materials should also be explored such as thermoelastic, viscoelastic, and other inelastic effects.

BIBLIOGRAPHY

[1] G. M. Baer, W. Small, T. S. Wilson, W. J. Benett, D. L. Matthews, J. Hartman, and D. J. Maitland. Shape memory behavior of thermally stimulated polyurethane for medical applications. *Journal of Applied Polymer Science*, 103:3882–3892, 2007.

[2] R. Beblo and L.M. Weiland. Light activated shape memory polymer characterization. *Journal of Applied Mechancics*, 76(1):011008, 2009.

[3] M. Behl and A. Lendlein. Shape-memory polymers. *Materials Today*, 10(4):20–28, 2007.

[4] McKinley G.H. Wilson T.S. Small Iv W. Benett W.J. Bearinger J.P. McElfresh M.W. Maitland D.J. Buckley, P.R. Inductively heated shape memory polymer for the magnetic actuation of medical devices. *IEEE Transactions on Biomedical Engineering*, 53(10):2075, 2006.

[5] S. Chandrasekhar. *Radiative Transfer*. Dover Publications inc.:, New York, NY, first edition, 1960.

[6] Y. C. Chen and D. C. Lagoudas. A constitutive theory for shape-memory polymers. part i. large deformations. *Journal of the Mechanics and Physics of Solids*, 56(2008):1752–1765, 2008.

[7] S. A. Chester, C. V Di Leo, and L. Anand. A finite element implementation of a coupled diffusion-deformation thoery for elastomeric gels. *International Journal of Solids and Structures*, 52:1–18, 2015.

[8] E.A. de Souza Neto, D. Perić, M. Dutko, and Owen. Design of simple low order finite elements for large strain analysis of nearly incompressible solids. *International Journal of Solids and Structures*, 33:3277–3296, 1996.

[9] G.E. Gurtin, E. Fried, and E. Anand. *The Mechanics and Thermodynamics of Continua*. Cambridge University Press:, New York, NY, first edition, 2010.

[10] G.A. Holzapfel. *Nonlinear Solid Mechanics A Continuum Approach For Engineering*. John Wiley and Sons Ltd.:, West Sussex, England, second edition, 2000.

[11] P. Houston, R. Rannacher, and S. Endre. A posteriori error analysis for stabilised nite element approximations of transport problems. *Computer Methods in Applied Mechanics and Engineering*, 90:1483–1508, 2000.

[12] T.J.R Hughes. *The Finite Element Method Linear Static and Dynamic Finite Element Analysis*. Dover Publications inc.:, New York, NY, second edition, 2008.

[13] H. Jiang, S. Kelch, and A. Lendlein. Polymers move in response to light. *Advanced Materials*, 18(11):1471, 2006.

[14] A. Lendlein, J. Hongyan, O. Junger, and R. Langer. Light-induced shape-memory polymers. *Nature*, 434(7035):879, 2005.

[15] A. Lendlein and R. Langer. Biodegradable, elastic shape-memory polymers for potential biomedical applications. *Science*, 296:1673–1676, 2002.

[16] K.N. Long, T.F. Scott, H.J. Qi, C.N. Bowman, and M.L. Dunn. Photomechanics of light-activated polymers. *Journal of the Mechanics and Physics of Solids*, 57:1103–1121, 2009.

[17] D. J. Maitland, M. F. Metzger, D. Schumann, A. Lee, and T. S. Wilson. Photothermal properties of shape-memory polymer micro-actuators for treating stroke. *Lasers in Surgery and Medicine*, 30:1–11, 2002.

[18] A. Metcalfe, A. Desfaits, and I. Salazkin. Cold hibernated elastic memory foams for endovascular interventions. *Biomaterials*, 24:491–497, 2003.

[19] M. F. Metzger, T. S. Wilson, D. Schumann, D. L. Matthews, and D. J. Maitland. Mechanical properties of mechanical actuator for treating ischemic stroke. *Biomedical Microdevices*, 4:89–96, 2002.

[20] S. Ota. A current status of irradiated heat-shrinkable tubing in japan. *Radiation Physics and Chemistry*, 18:81–87, 1981.

[21] H. J. Qi, Castro F. Nguyen, T. D., C. M. Yakacki, and R. Shandas. Finite deformation thermo-mechanical behavior of thermally induced shape-memory polymers. *Journal of the Mechanics and Physics of Solids*, 56(2008):1730–1751, 2008.

[22] J.S. Sodhi, P.R. Cruz, and I.J. Rao. Inhomogeneous deformations of light activated shape memory polymers. *International Journal of Engineering Science*, 89:1–17, 2014.

[23] J.S. Sodhi and I.J. Rao. Modeling the mechanics of light activated shape memory polymers. *International Journal of Engineering Science*, 48(11):15761589, 2010.

[24] V. Srivastava, S. A. Chester, and L. Anand. Thermally actuated shape-memory polymers: Experiments, theory, and numerical simulations. *Journal of the Mechanics and Physics of Solids*, 58(8):1100–1124, 2010.

[25] P. Vettiger, G. Cross, M. Despont, U. Drechsler, U. Düring, B. Gotsmann, W. Häberle, M. A. Lantz, Stutz R. Rothuizen, H. E., and G. K. Binning. The millipedenanotechnology entering data storage. *IEEE Transactions on Nanotechnology*, 1(2002):39–55, 2002.

[26] E. Wornyo, K. Gall, F. Yang, and W. King. Nanoindention of shape-memory polymer networks. *Polymer*, 48(2007):3213–3225, 2007.

[27] P. Wriggers. *Nonlinear Finite Element Methods*. Springer-Verlag, Berlin, Germany, first edition, 2008.